Optimal Closed-Loop Approaches in Flow Control

Rudibert King
Berlin Institute of Technology ER2-1, Department of Process and Plant Technology, Hardenbergstr. 36a, D-10623 Berlin, Germany

Abstract Different experimentally validated procedures to synthesize closed-loop flow controllers are presented which use the solution of an optimization problem in various ways. The controller synthesis or the control laws itself are based on the knowledge of low dimensional models. These range from Galerkin systems as introduced in other chapters of this volume and identified black-box models to the most simplest process model which only assumes that some kind of extremum exists. Numerous experimental results show the power of extremum seeking control, robust control or model predictive control in closed-loop flow control applications.

1 Introduction

In addition to the methods shown in the chapter by L. Cordier optimal approaches are presented here which do not need the solution of a system of adjoint equations. They focus on the synthesis of closed-loop control systems in contrast to the open-loop nature of the aforementioned Hamiltonian approach. By this, the robustness concerning unavoidable disturbances acting on the fluid flow and model uncertainties entering the control law and existing in every low dimensional model is greatly enhanced. A selection of control concepts is introduced which uses optimization-based steps in different aspects and different levels. In model predictive control a value function considering the future behavior of a process will be minimized either analytically in an unconstrained or numerically in a constrained case. In extremum seeking control and its generalization slope seeking a gradient-based minimization or maximization is exploited which is purely based on online available experimental data. Robust control minimizes an H_∞-norm to guarantee robust stability, robust performance and to limit the control energy spend.

Some of the methods introduced rely on low dimensional models which are set up to describe the input-output behavior of a process in a black-box

manner. Here, the central task in model identification is the solution of an optimization problem to determine model parameters. Galerkin systems, which are considered as well, may need a calibration of model parameters which again goes back to an optimization problem. Hence, optimization methods are abounded in closed-loop control engineering science in general and in particular in closed-loop flow control.

Although fluid flow systems as described by the Navier-Stokes equation are inherently nonlinear much can be achieved in closed-loop control exploiting linear concepts. This partly stems from the fact that in some applications a controller tries to keep the process near an operating point around which a linearization gives a good approximation. Moreover, the basic reason for applying closed-loop control is tackling uncertainty. If no disturbances would act on a process and the process could be completely described by a model (which can be solved online) open-loop concept would suffice. As these assumptions will never be valid outside a simulation study closed-loop control is a must and uncertainties coming from only roughly approximating linear model can be tolerated. For this, § 2 recapitulates some basic facts about linear systems and system identification. Different controllers are introduced next starting with the most simple extremum seeking-type of approach in § 3.1. Linear models are then used in the synthesis of robust and state space controllers in § 3.2. For model-based estimation techniques necessary to implement such controllers the reader is referred to the chapter of G. Tadmor in this volume. Finally, different nonlinear controllers, especially model predictive controllers (MPC) are considered in § 3.3. Here the Galerkin system of the flow around a circular cylinder which is used in other chapters as well will be used inside a MPC scheme. Various real-life applications are given in § 4 before a comparison is presented in § 5.

A special word is necessary concerning nomenclature in flow control as two formerly distinct disciplines, namely fluid mechanics and control engineering, meet. As a consequence different important variables in the respective disciplines are given the same symbols. Most notably $\mathtt{u}$, i.e. $\mathtt{u} = \mathtt{u}(t)$, relates to the (scalar) control input / plant input / manipulated variable in control whereas it represents the time- and space-dependent velocity fluctuation $u = u(t, x, y, z)$ in fluid mechanics. As this chapter would be almost the only one in this book using its own nomenclature and to help the reader who is new both to low dimensional modeling **and** control an adaptation of the control engineering nomenclature to the fluid mechanics notation would make sense. However, many good arguments exist as well for using the control engineering notation in this chapter. To name just a few: 1) Somebody working in an interdisciplinary field must know and understand the

meaning of double used symbols from the actual context. 2) This chapter cannot give a comprehensive introduction in control. Therefore, the reader has to be referred to control engineering textbooks and articles quite often which use the standard control engineering notation anyway. 3) This chapter summarizes some of the ideas which had been followed by the authors' group in the last 10 years. Not all details will be repeated here. Instead, references are made to different articles where details can be found given again in control notation. 4) Only very few symbols will be redefined here in comparison to the rest of the book and will be typeset in a teletype style which should help reading. A comparison of some important variables is given in Table 1 to help cross-references.

symbol	control	symbol	fluid mechanics
$\mathtt{s}$	Laplace variable	$\mathbf{s}$	sensor signal
$\mathtt{u}$	plant input, $\mathtt{u} \in \mathbb{R}^1$	u	streamwise velocity fluctuation
$\mathbf{u}$	plant input, $\mathbf{u} \in \mathbb{R}^p$	$\boldsymbol{u}$	$= (u, v, w)$ velocity field
$\mathbf{x}$	state, $\mathbf{x} \in \mathbb{R}^n$	$\mathbf{x}$	unit vector
$\mathtt{y}$	plant output, $\mathtt{y} \in \mathbb{R}^1$	y	wall-normal coordinate
$\mathtt{y}$	plant output, $\mathbf{y} \in \mathbb{R}^q$		

Table 1. Important symbols in control and fluid mechanics. Control related symbols will be used in this chapter.

2 Linear systems

Irrespective whether the flow around a bluff body, an aircraft wing, see Fig. 1, in a turbomachine or the flow and combustion in a burner is considered, an input-output point of view can be adopted for several approaches in control. In all cases the system involved reacts to some flow control inputs, such as periodic blowing or suction, acoustic actuation, magneto-hydrodynamic forces, by an application-defined output signal. For the bluff body and the wing it could be drag and/or lift. In turbomachines the noise emitted might be the interesting output signal in one application and the pressure increase over a compressure stage in another. The focus in a burner study might be on pressure fluctuations from a thermo-acoustic instability or on the NO_x-production. Hence, the output has to be newly defined for every new application.

In the single-input-single-output (SISO) case with a scalar input $\mathtt{u}(t)$ and a scalar output $\mathtt{y}(t)$, a linear system can be described by an n-th order

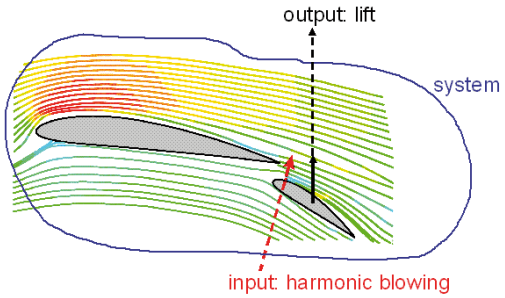

Figure 1. Wing with flap viewed as a system. The size of a harmonic blowing at the leading edge of the flap is chosen as the input and the lift force as output signal.

ordinary linear differential equation with constant coefficients

$$\begin{aligned} a_n \overset{(n)}{\mathtt{y}}(t) \quad &+a_{n-1} \overset{(n-1)}{\mathtt{y}}(t) + \cdots + a_1 \dot{\mathtt{y}}(t) + a_0 \mathtt{y}(t) \\ &= b_0 \mathtt{u}(t) + b_1 \dot{\mathtt{u}}(t) + \cdots + b_m \overset{(m)}{\mathtt{u}}(t) \end{aligned} \tag{1}$$

and appropriate initial conditions. For implementation of algorithms in real-time and for system identification a discrete-time version of this equation is more appropriate. The most simplest although not best version starting from Eq. (1) would be an approximation of the differential operators by difference operators, such as

$$\dot{\mathtt{y}}(t)|_{t=kT} \approx \frac{\mathtt{y}(kT) - \mathtt{y}((k-1)T)}{T} = \frac{\mathtt{y}_k - \mathtt{y}_{k-1}}{T} \tag{2}$$

with sampling period T yielding

$$\mathtt{y}_k + \alpha_1 \mathtt{y}_{k-1} + \cdots + \alpha_n \mathtt{y}_{k-n} = \beta_1 \mathtt{u}_k + \beta_2 \mathtt{u}_{k-1} + \ldots \beta_m \mathtt{u}_{k-m+1} \quad . \tag{3}$$

As a result, the output at the (actual) time k can be expressed as a function of old outputs and old and actuals controls $\mathtt{u}_{k-j}$, $j = 0, 1, \ldots, m-1$.

$$\mathtt{y}_k = -\alpha_1 \mathtt{y}_{k-1} - \cdots - \alpha_n \mathtt{y}_{k-n} + \beta_1 \mathtt{u}_k + \beta_2 \mathtt{u}_{k-1} + \ldots \beta_m \mathtt{u}_{k-m+1} \quad . \tag{4}$$

For systems from fluid mechanics an additionally pure time-delay d, i.e. $T_0 = dT$, is very often observed between input and output leading to

$$\begin{aligned} \mathtt{y}_k = \quad &-\alpha_1 \mathtt{y}_{k-1} - \cdots - \alpha_n \mathtt{y}_{k-n} \\ &+\beta_1 \mathtt{u}_{k-d} + \beta_2 \mathtt{u}_{k-d-1} + \ldots \beta_m \mathtt{u}_{k-d-m+1} \quad . \end{aligned} \tag{5}$$

Hence, the actual input does not directly influence the actual output. This time-delay is affected by the convection time between the location of the actuator and the position of the sensor.

Introducing the shift operator q with $\mathtt{y}_{k-1} = q^{-1}\mathtt{y}_k$ and $\mathtt{y}_{k-\nu} = q^{-\nu}\mathtt{y}_k$ gives

$$(1 + \alpha_1 q^{-1} + \cdots + \alpha_n q^{-n})\mathtt{y}_k = (1 + \beta_1 q^{-1} + \cdots + \beta_m q^{-m+1})q^{-d}\mathtt{u}_k$$

which can be formally solved for the actual output

$$\mathtt{y}_k = \frac{1 + \alpha_1 q^{-1} + \cdots + \alpha_n q^{-n}}{1 + \beta_1 q^{-1} + \cdots + \beta_m q^{-m+1}} q^{-d}\mathtt{u}_k = G(q^{-1})\mathtt{u}_k \quad . \tag{6}$$

Hence, the output can be written as the input signal $\mathtt{u}_k$ times a discrete time transfer function $G(q^{-1})$.

The same input-output behavior is described by a state-space model which is given first in the continuous time domain

$$\begin{aligned} \dot{\boldsymbol{x}}(t) &= \boldsymbol{A}'\boldsymbol{x}(t) + \boldsymbol{b}'\mathtt{u}(t) \ , \quad \boldsymbol{x}(t_0) = \boldsymbol{x}_0 & (7)\\ \mathtt{y}(t) &= \boldsymbol{c}^T\boldsymbol{x}(t) + d\mathtt{u}(t) & (8) \end{aligned}$$

with[1] $\boldsymbol{x} \in \mathbb{R}^n$. For the simple example

$$\overset{(3)}{\mathtt{y}}(t) + 3\overset{(2)}{\mathtt{y}}(t) + 2\dot{\mathtt{y}}(t) + 5\mathtt{y}(t) = 2\mathtt{u}(t)$$

chose for example $\mathtt{x}_1 \equiv \mathtt{y}$, $\mathtt{x}_2 \equiv \dot{\mathtt{y}}$ and $\mathtt{x}_3 \equiv \ddot{\mathtt{y}}$ to obtain

$$\begin{aligned} \dot{\boldsymbol{x}}(t) &= \begin{pmatrix} 0 & 1 & 0 \\ 0 & 0 & 1 \\ -5 & -2 & -3 \end{pmatrix}\boldsymbol{x}(t) + \begin{pmatrix} 0 \\ 0 \\ 1 \end{pmatrix}\mathtt{u}(t) \\ \mathtt{y}(t) &= (1 \ 0 \ 0)\boldsymbol{x}(t) \end{aligned} \tag{9}$$

with appropriate initial conditions. If derivatives of the input appear on the right hand side of Eq. (1), more involved transformations are necessary, see standard control engineering textbooks or refer to standard control engineering software such as MATLAB®.

In the multiple-input-multiple-output (MIMO) case the state-space model reads without a time-delay between input and output

$$\begin{aligned} \dot{\boldsymbol{x}}(t) &= \boldsymbol{A}'\boldsymbol{x}(t) + \boldsymbol{B}'\boldsymbol{u} & (10)\\ \boldsymbol{y} &= \boldsymbol{C}\boldsymbol{x}(t) + \boldsymbol{D}\boldsymbol{u} \quad . & (11) \end{aligned}$$

[1] $\boldsymbol{A}'$, $\boldsymbol{B}'$, $\boldsymbol{b}'$ refer to a continuous-time model while $\boldsymbol{A}$, $\boldsymbol{B}$, $\boldsymbol{b}$ are used in a discrete-time version below. The transpose of a matrix is dended by ^{T}.

In this case an exact discrete-time description is obtained for systems with piecewise constant inputs, i.e. $\boldsymbol{u} = \boldsymbol{u}(k) = \text{const.}$ for $kT \leq t < (k+1)T$, using the general solution of Eq. (10)

$$\boldsymbol{x}(t) = e^{\boldsymbol{A'}(t-t_0)}\boldsymbol{x}_0 + \int_{t_0}^{t} e^{\boldsymbol{A'}(t-\tau)}\boldsymbol{B'}\boldsymbol{u}(\tau)d\tau \quad . \tag{12}$$

Then, the discrete version reads

$$\boldsymbol{x}(k+1) = \boldsymbol{A}\boldsymbol{x}(k) + \boldsymbol{B}\boldsymbol{u}(k) \tag{13}$$

$$\boldsymbol{y}(k) = \boldsymbol{C}\boldsymbol{x}(k) + \boldsymbol{D}\boldsymbol{u}(k) \tag{14}$$

with

$$\boldsymbol{A} = e^{\boldsymbol{A'}T} \quad , \quad \boldsymbol{B} = \int_0^T e^{\boldsymbol{A'}(T-\tau)}\boldsymbol{B'}d\tau = (\boldsymbol{A'})^{-1}(\boldsymbol{A} - \boldsymbol{I})\boldsymbol{B'}$$

and an identity matrix $\boldsymbol{I}$ of appropriate dimension.

Stability of the open-loop system is given when all eigenvalues of $\boldsymbol{A'}$ or $\boldsymbol{A}$ stay in the open left half complex plane in the time continuous case or in the unit circle in the discrete-time case, respectively.

Classical control is often done in the Laplace or frequency domain. Applying the Laplace transformation with complex variable $\mathtt{s} = \sigma + j\omega$

$$L\{\mathtt{f}(t)\} = \mathtt{f}((\mathtt{s})) = \int_0^\infty \mathtt{f}(t)e^{-(\mathtt{s})t}dt \tag{15}$$

to Eq. (1) for vanishing initial conditions yields

$$\mathtt{y}(\mathtt{s}) = G(s)\mathtt{u}(s) \tag{16}$$

with the transfer function $G(\mathtt{s})$ which is now given in the Laplace domain

$$G(\mathtt{s}) = \frac{b_0 + b_1\mathtt{s} + \cdots + b_m s^m}{a_0 + a_1\mathtt{s} + \cdots + a_n\mathtt{s}^n} \quad .$$

Hence, the input-output behavior of a dynamic system can be described by a simple multiplication of the transformed input $\mathtt{u}(\mathtt{s})$ by the transfer function $G(\mathtt{s})$. This will ease the treatment of the closed loop, see below.

Applying the Laplace transformation to Eq. (7) and Eq. (8) shows the relation between the two sorts of system descriptions

$$G(\mathtt{s}) = \boldsymbol{c}^T(\mathtt{s}\boldsymbol{I} - \boldsymbol{A'})^{-1}\boldsymbol{b'} + d \quad . \tag{17}$$

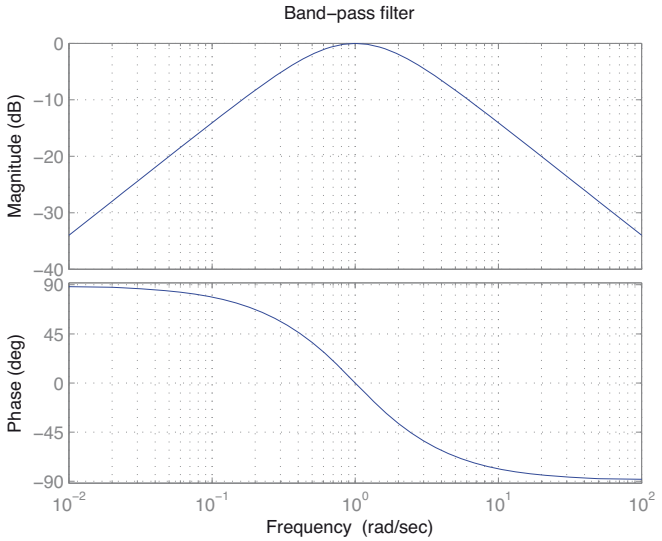

Figure 2. Bode plot of a band-pass filter of second order $G(j\omega) = Kj\omega\omega_2/[(j\omega+\omega_1)(j\omega+\omega_2)]$ with $\omega_1 = \omega_2 = 10$rad/sec and $K = 2$. Observe that for $\omega = \omega_1 = \omega_2$ no damping and no phase shift occurs. However, slower and faster components are dampened.

If $\mathtt{s} = j\omega$, the frequency response $G(j\omega)$ is obtained which gives a frequency-dependent gain, $|G(j\omega)|$, and phase-shift, $\arg\{G(j\omega)\}$, between input and output for sinusoidal inputs. A graphical representation is given in the Bode plot in which $20\log_{10}|G(j\omega)|$, the so-called magnitude, and the phase $\arg\{G(j\omega)\}$ are plotted as a function of $\omega = 2\pi f$, cf. Fig. 2.

If the linear model is not obtained through linearization of a given nonlinear model of the flow, for example a Galerkin system, it has to be identified from experiments in a black-box approach. In this case the real flow around a setup is replaced, conceptually, by a black-box for which only an input-output relation has to be determined. Such a black-box will present in the high-lift device introduced above only the relation between the actuation amplitude $\mathtt{u}(t)$ and the mean lift. As the mean lift cannot be measured on a real wing a surrogate output variable can be defined in this example. It is well known, cf. Becker et al. (2007), that a relation exists between the lift and a pressure difference along the suction side of the wing or flap. This signal will be defined as the surrogate output. No information about

flow velocity, vorticity, etc. will be contained in such model. Nor will it be able to predicted for example the drag imposed on the wing. However, this model will suffice completely if only the lift has to be controlled.

To *identify* a black-box model, the system is excited by appropriate input signals $\mathtt{u}(t)$. Most often step-wise changes in the control input are used, see Fig. 4. These are easy to analyze. However, a theoretical study shows that the information content in the answer to a step input is limited in the frequency range. A better input signal is a pseudo random binary signal (PRBS) which consists of many step-ups and step-downs in an almost random fashion, see Ljung (1999) for more details and Fig. 3.

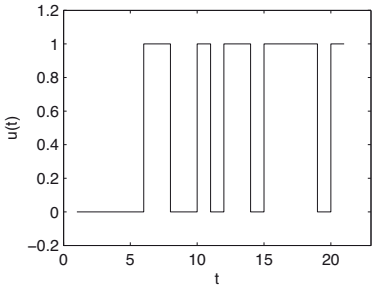

Figure 3. PRBS-signal with unity amplitude. Fourier analysis shows that this signal contains many discrete frequencies. It is used instead of a white noise process as an excitation signal in identification. A white noise would possess a continuum of all frequencies with the same intensity which would be good for identification of an unknown system. However, as its energy content would be infinity, a white noise process does not exist and is replaced by this deterministic sequence.

The coefficients α_i, β_j and the dimensions and time-delay n, m and d, respectively, of the time-discrete model Eq. (5) are then estimated in general by the solution of the following optimization problem

$$\min_{\alpha_i,\beta_j,n,m,d} \sum_{l_e} \sum_{k} w_{l_e k} (\mathtt{y}_k^{(l_e)} - \tilde{y}_k^{(l_e)})^2$$

where l_e runs over all experiments used, k indicates individual instants and $w_{l_e k}$ are weights to improve identification. The real measurements are denoted by $\mathtt{y}$. Measurements calculated by the model, $\tilde{\mathtt{y}}$, depend on the design variables of the optimization problem, i.e. $\tilde{\mathtt{y}}_k = \tilde{\mathtt{y}}_k(\alpha_i, \beta_j, n, m, d)$. Care has to be taken concerning unavoidable noise present in every experiment. Only

if the influence of this noise is included in a correct fashion in identification as it is done for example in so-called prediction-error-methods, good parameter estimates are obtained. More information about system identification can be found in Ljung (1999).

After a time-discrete model is identified it can be transformed to a continuous-time form, either to a transfer function $G(\mathtt{s})$ or to the state-space matrices $\boldsymbol{A}'$, $\boldsymbol{B}'$, $\boldsymbol{C}$ and $\boldsymbol{D}$. The latter can be identified directly as well by subspace methods, see Ljung (1999). Fig. 4 shows a comparison between measured data and a simulation of an identified model for a step-wise excitation. In this case a rather simple flow, namely the flow over a backward-facing step, is considered. Despite its simplicity, a rich dynamic can be observed in the right panel of Fig. 4 on the one hand. On the other hand an input-output view with a restriction to the reattachment length as the output signal shows a very simple input-output behavior which suffice for controller synthesis.

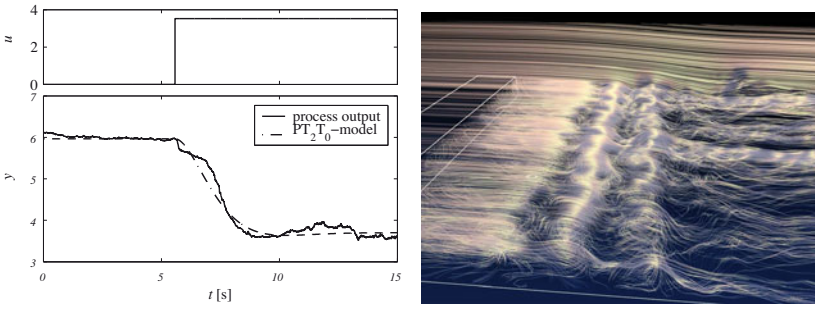

Figure 4. Left: Comparison of the measured reattachment length behind a backward-facing step (solid line) and a fit with a second order model with time delay, $G(\mathtt{s}) = b_0/(1 + a_1\mathtt{s} + a_2\mathtt{s}^2)e^{-dT\mathtt{s}}$, see King et al. (2004). Right: Illuminated stremalines of a LES of the flow around a backward-facing step from Weinkauf et al. (2003)

3 Methods in closed-loop control

Various methods of control are introduced starting with model-free approaches in § 3.1. A recapitulation of classical linear control and robust control is summarized in § 3.2. Finally, § 3.3 gives details about nonlinear approaches including model predictive control.

3.1 Extremum and slope seeking control

The following section is adopted from Henning et al. (2008) where more information can be found. Extremum- and slope-seeking feedback controllers are adaptive gradient-based, model-independent feedback schemes that search for optimal actuation parameters (Garwon et al., 2003; Beaudoin et al., 2006; Henning et al., 2007). The only (extremely low dimensional) modeling concept used, though not explicitly stated in the sense of an equation, is the knowledge that some kind of extremum in an input-output map exists. An extremum-seeking control can be used to find areas around distinct minima or maxima in the steady-state map of a plant. As many flow applications are rather characterized by a plateau-type map, slope-seeking is better suited. Here, the system is driven to a preset reference slope which is representative for a value just below the plateau. Two different configurations are used in this study, a single SISO and a multiple SISO slope-seeking controller. Extensions to the truly multiple input case can be found in King et al. (2006). As the extremum-seeking controller forms the basis for the slope-seeking variant, the former is reviewed first.

Classical extremum seeking control Extremum-seeking control is an effectively model-free method for the control of nonlinear plants characterised by an output extremum in the steady-state (Morosanov, 1957; Krstic and Wang, 2000; Ariyur and Krstic, 2003) and for linear or nonlinear plants for which the output is defined as the norm of the difference between a reference value $r(t)$ and the plant output y, e.g. $(r(t) - \mathtt{y}(t))^2$ in a SISO-setting. Typical examples in flow control are the maximizations of the lift of a wing or the mixing in a burner, the minimizations of the drag of a car or the noise emitted in a turbomachine. As every minimisation problem can easily be transformed into a maximisation problem, all explanations are given for the latter case. The Fig. 5 shows the structure of the basic SISO extremum-seeking control loop. Here, the process is described by both, it's steady-state map $\mathtt{y}_s = f(\mathtt{u}_s)$ and it's dynamical model for ease of further discussion.

The idea of this gradient based method is an on-line optimisation of the average value, $\mathtt{u}_s$, of the control input $\mathtt{u}(t)$ such that the average of the output equals the maximum steady-state value, $\mathtt{y}_s = \mathtt{y}_s^*$. With extremum-seeking control this can be accomplished without knowing the steady-state input-output map $\mathtt{y}_s = f(\mathtt{u}_s)$. The controller works as follows: Assume that the initial control input $\mathtt{u}_0'$, see Fig. 5, which is calculated by some higher level control hierarchy, see below, and a slowly changing part $\Delta\mathtt{u}(t)$, i.e. $\mathtt{u}_0' = \mathtt{u}_0 + \Delta\mathtt{u}(t)$, are superimposed with a sinusoidal signal $\mathtt{a}\sin(\omega_{sin}t)$

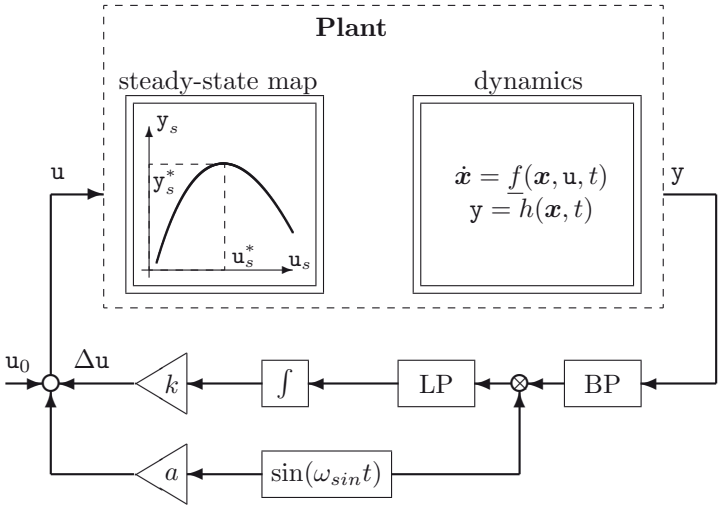

Figure 5. Block diagram of closed-loop extremum-seeking. The BP and LP represent band- and low-pass filters, respectively. Both the steady state map and the nonlinear dynamic system representation are given for the same plant.

which has a small amplitude $\mathtt{a}$.

$$\mathtt{u}(t) = \mathtt{u}_0 + \Delta\mathtt{u}(t) + \mathtt{a}\sin(\omega_{sin} t) \tag{18}$$

If the period of this harmonic perturbation is larger than the largest time constant of the process, the output of the process will also be approximately sinusoidal, centred initially around $\mathtt{y}_{s,0} = f(\mathtt{u}_0')$. Likewise, the amplitude will be approximately af'. Hence,

$$\mathtt{y}(t) \approx \mathtt{y}_s + \mathtt{a}f'\sin(\omega_{sin} t) \quad . \tag{19}$$

This output perturbation is analysed in order to detect the slope (gradient) of the input-output map which is used for gradient based optimisation. To do this, the mean value $\mathtt{y}_s$ is removed by a band-pass filter (BP), for example of second order[2]

$$G_{BP}(j\omega) = \frac{j\omega\omega_2}{(j\omega + \omega_1)(j\omega + \omega_2)} \quad , \tag{20}$$

[2]A high-pass filter was proposed originally. However, for flow control with rather noisy measurements a BP is recommended.

with the lower cut-off frequency ω_1 and the upper cut-off frequency ω_2, see as well Fig. 2. By application of a BP the output of the filter reads

$$\mathtt{y}_{BP}(t) \approx |G_{BP}(j\omega_{sin})|\, af' \sin(\omega_{sin}t + \varphi_{BP}) \quad . \tag{21}$$

The product $\mathtt{y}_P(t)$ of this filtered output and the zero-mean sine signal $\sin(\omega_{sin}t)$ indicates the slope of the unknown map $\mathtt{y}_s = f(\mathtt{u}_s)$:

$$\begin{aligned} \mathtt{y}_P(t) &= \sin(\omega_{sin}t)\Big(|G_{BP}(j\omega_{sin})|\, af' \sin(\omega_{sin}t + \varphi_{BP})\Big) \\ &= |G_{BP}(j\omega_{sin})|\, af' \times \\ &\times \Big(\sin^2(\omega_{sin}t)\cos(\varphi_{BP}) + \sin(\omega_{sin}t)\cos(\omega_{sin}t)\sin(\varphi_{BP})\Big) \quad . \end{aligned} \tag{22}$$

This product leads to a non-zero mean signal obtained with a low-pass filter (LP), see Fig. 5, as long as the maximum is not obtained. If the plant is initially to the left of the maximum, the input and output perturbations are in phase, that is the product will be positive, see as well Fig. 6. An

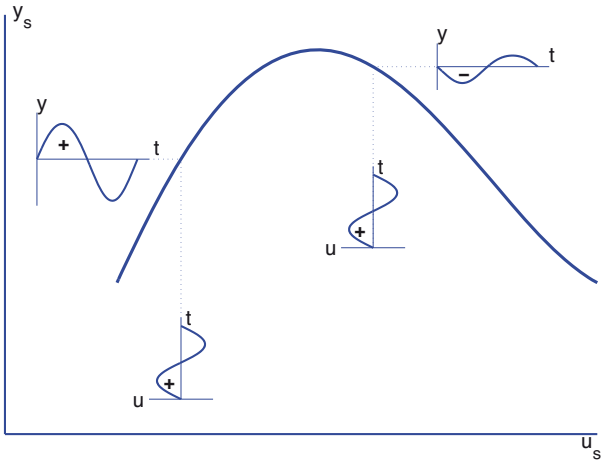

Figure 6. Sketch of a nonlinear static map and quasi-steady state responses when the sinusoidal input $\mathtt{u}$ is either on the left or right hand side of the maximum. Only the offset-free part of the output $\mathtt{y}$ obtained after the BP is depicted.

anti-phase relation which gives a negative product is an indication that the plant is on the right of the maximum. To see this, approximate the output $\mathtt{y}_{LP}(t)$ of the LP by an average calculated for one period $T = 2\pi/\omega_{sin}$, that is

$$\begin{aligned} \mathtt{y}_{LP}(t) &\approx \frac{1}{T}\int_0^T \mathtt{y}_P(t)dt \\ &= \frac{1}{T}|G_{BP}(j\omega_{sin})|\,\mathtt{a}f'\,\frac{T}{2}\cos(\varphi_{BP}) \\ &= \frac{\mathtt{a}f'}{2}\Re\{G_{BP}(j\omega_{sin})\} \quad . \end{aligned} \tag{23}$$

With this information an additional term $\Delta\mathtt{u}(t)$, added to $\mathtt{u}_0 + \mathtt{a}\sin\omega_{sin}t$, see Eq. (18) and Fig. 5, is calculated by time integration and multiplication by k. As long as the output of the LP is positive, that is the system is on the left side of the maximum, a steadily increasing control input $\mathtt{u}$ is obtained. For a negative output of the LP, the opposite is true. The adaptation of $\mathtt{u}$ converges to $\mathtt{u} = \mathtt{u}^*$.

The constant $\mathtt{u}_0$ is set by the user to a value for which a non-zero gradient is expected. If this value is chosen too low, for example, the flow system will not react to the variation of the input signal. Hence, no reliable operation is guaranteed.

The extremum-seeking scheme is an adaptive closed-loop type of control. It guarantees closed-loop stability if designed properly, see Krstic and Wang (2000) and Ariyur and Krstic (2003) for details. The choice of certain design parameters determines the speed of convergence. For the results given below we chose $\omega_{BP} = \omega_1 = \omega_2 = \omega_{sin}$. The LP is not necessary, but it is helpful in filtering out the perturbation after the multiplier. Therefore, the cut-off frequency of the LP should be chosen to $\omega_{LP} \leq \omega_{sin}$. In addition, the adaption gain k needs to be small. If the plant behaviour varies due to uncertainties, the time scale of the perturbation signal has to be slower than the slowest possible plant dynamic. The main advantage of this extremum-seeking control is that no plant model is needed for controller synthesis. However, the control suffers from both, the permanent harmonic input and output perturbations, and the relative slow dynamic behaviour. Therefore, some extensions will be proposed later.

Slope seeking control In flow control, situations are encountered in which the static input-output map does not show a distinct maximum. Instead it is characterised by a plateau-type behaviour as illustrated in Fig. 7. A detached flow over an aircraft wing, to give an example, can be influenced by active flow control such that it reattaches again. At some point,

however, the flow is completely attached. A further increase of the control input will not result in a further increase nor in a decrease of the lift. The extremum-seeking control described above will work correctly in this situation if it starts left of the plateau. However, when the control input is larger than the smallest value necessary to be on top of the plateau, it will not be minimised. Such a waste of control energy can be observed likewise when the system's behaviour - due to a change in operating conditions - will change. In such a case, the plateau-type map might be shifted to the left. The smallest value necessary to be on top of the plateau found for the last operating condition now lays somewhere on the plateau without any gradient information for the controller. To tackle such systems, slope-seeking is considered next.

The slope-seeking is an extension of the extremum-seeking scheme, for details see Ariyur and Krstic (2003). It drives the plant output to a value that corresponds to a reference slope of the steady-state input-output-map:

$$f'_{ref} = \left.\frac{\partial \mathtt{y}_s}{\partial \mathtt{u}_s}\right|_{ref} . \tag{24}$$

Therefore, according to Eq. (23), a negative reference value

$$r(f'_{ref}) = -\frac{\mathtt{a}\, f'_{ref}}{2} \Re\left\{G_{BP}(j\omega_{sin})\right\}, \tag{25}$$

as a function of f'_{ref} is added to the actually detected slope, see Fig. 7. Thus, the apparent extremum is shifted. Since extremum-seeking is a special case of slope-seeking, when the reference slope is zero, designing the filters, the integrator gain, and the sinusoidal perturbation are the same.

Increase of bandwidth Different methods to improve extremum- and slope-seeking control are given in Henning et al. (2008). A very powerful modification to speed-up the closed-loop behavior will be shown in the sequel. In the meantime this approach has been used in turbomachines, in an industrial high-lift design, bluff bodies and burner studies to accelerate settling time by a factor of 3-9.

As in the classical extremum-seeking control we still assume that the harmonic perturbation of the process is slower than the slowest time constant of the process. Hence, the static input-output map is reflected by the behaviour of the output $\mathtt{y}(t)$. If the input perturbation $\mathtt{a}$ is small enough, the output perturbation should be $\mathtt{a}f'$, as already mentioned in Sec. 3.1. The output itself consists of an approximately constant value plus this perturbation, that is

$$\mathtt{y}(t) \quad \approx \quad \mathtt{y}_s + \mathtt{a}f' \sin(\omega_{sin} t) \quad .$$

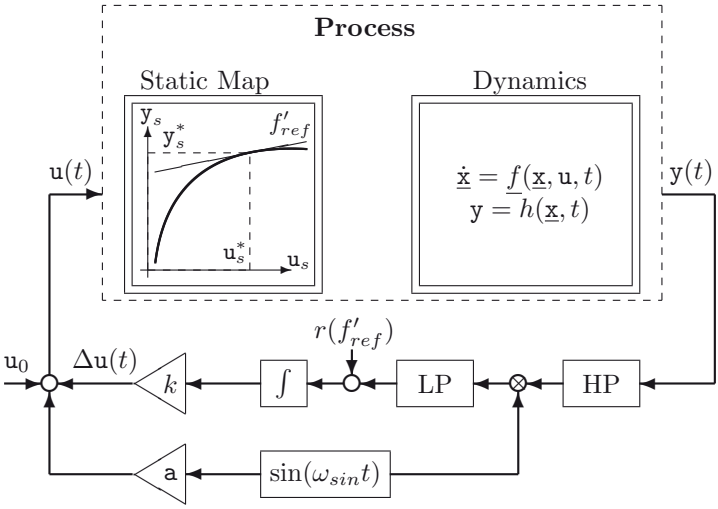

Figure 7. Block diagram of closed-loop slope-seeking.

With Eq. (18)

$$\begin{aligned} \mathtt{y}(t) &\approx \underbrace{\mathtt{y}_s - f'\mathtt{u}_0 - f'\Delta\mathtt{u}(t)}_{\mathtt{x}_1} + \underbrace{f'}_{\mathtt{x}_2}\mathtt{u}(t) \\ &= \mathtt{x}_1 + \mathtt{u}(t)\mathtt{x}_2 \quad . \end{aligned} \tag{26}$$

The idea is to observe these two parameters $\mathtt{x}_1$ and $\mathtt{x}_2$. A dynamical model for the two parameters reads in discrete time

$$\boldsymbol{x}(t_{k+1}) = \begin{bmatrix} 1 & 0 \\ 0 & 1 \end{bmatrix} \boldsymbol{x}(t_k) + \boldsymbol{w}_k \quad . \tag{27}$$

If Eq. (26) is used as a measurement equation, an observability analysis shows that $\mathtt{x}_1$ and $\mathtt{x}_2$ are not observable. However, when time-shifted input-output pairs $(\mathtt{u}(t), \mathtt{y}(t))$ and $(\mathtt{u}(t-n\Delta t), \mathtt{y}(t-n\Delta t))$ are considered, observability is given. With $\mathtt{y}_1(t_k) = \mathtt{y}(t_k)$ and $\mathtt{y}_2(t_k) = \mathtt{y}(t_{k-n})$ the measurement equation now reads

$$\boldsymbol{y}(t_k) = \begin{bmatrix} 1 & \mathtt{u}_1 \\ 1 & \mathtt{u}_2 \end{bmatrix} \boldsymbol{x}(t_k) + \boldsymbol{v}_k \tag{28}$$

with $\mathtt{u}_1 = \mathtt{u}(t_k)$ and $\mathtt{u}_2 = \mathtt{u}(t_{k-n})$. The vectors $\boldsymbol{w}_k$ and $\boldsymbol{v}_k$ denote Gaussian white noises. An extended Kalman filter (Gelb, 1986) can be used for

real-time estimation of the states. The modification of the slope-seeking control by inclusion of this model-based sensor is shown in Fig. 8. Since the extended Kalman filter estimates the slope $\hat{f}' = \hat{\mathtt{x}}_2$, the reference slope f'_{ref} is subtracted directly from $\hat{f}'$.

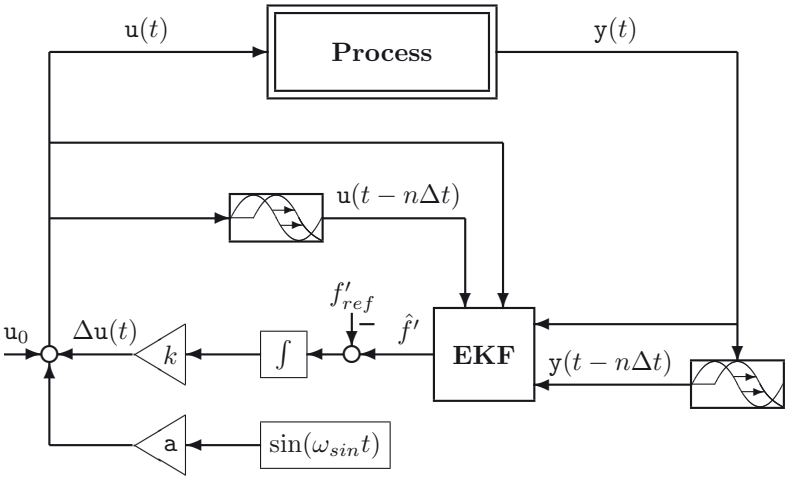

Figure 8. Block diagram of the closed-loop slope-seeking with an extended Kalman filter (EKF) algorithm for fast real-time estimation of the local gradient of the steady-state map.

3.2 Linear and robust control

For linear systems using the Laplace domain it is very easy to describe the output of a closed loop as a function of its inputs, see Fig. 9. For the scalar case the system output $y(s)$ is given by

$$\begin{aligned} \mathtt{y}(s) &= \frac{C(s)P(s)}{1+C(s)P(s)}\mathtt{r}(s) - \frac{C(s)P(s)}{1+C(s)P(s)}\mathtt{m}(s) + \frac{G_d(s)}{1+C(s)P(s)}\mathtt{d}(s) \\ &= T(s)\mathtt{r}(r) - T(s)\mathtt{m}(s) + S(s)\mathtt{d}(s) \end{aligned} \tag{29}$$

depending on the transfer functions $C(s)$, $P(s)$ and $G_d(s)$ of the controller, the plant and the disturbance coupling, respectively. Measurement noise is given by $\mathtt{m}$ and the other disturbances by $\mathtt{d}$.

In flow control applications the identification of local linear models around an operating point applying different step heights give rise to a family of different models reflecting the nonlinearity of the process. Quite often, a main

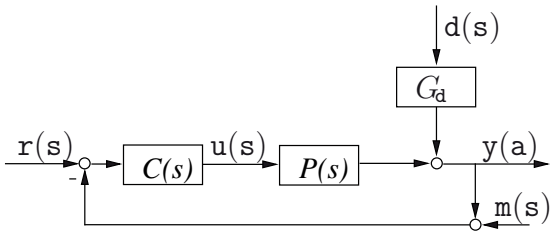

Figure 9. General closed loop with controller $C(s)$, plant $P(s)$, disturbance transfer function $G_d(s)$, reference $\mathtt{r}(s)$, disturbances $\mathtt{d}(s)$ and $\mathtt{m}(s)$ and system output $\mathtt{y}(s)$.

difference in these linear models can be seen in the gain of the identified models $P(s)$

$$K = P(s = 0) = \frac{b_0}{a_0} \quad .$$

which can be approximated as a function of the step height $\hat{\mathtt{u}}$ used, i.e. $K = f(\hat{\mathtt{u}})$. Physically, this reflects the situation that for example in the case of the high-lift device the lift force will not continuously increase when the actuation amplitude is increased. At some point the separated flow which is responsible for a reduced lift will completely reattach and any further increase in actuation will not result in any improvement. Hence, the ratio between increase in lift to actuation amplitude will decrease with increasing $\hat{\mathtt{u}}$.

Exploiting this knowledge, the degree of nonlinearity can be reduced by post-multiplying the calculated control signal $\mathtt{u}^*(t)$ by the inverse of f. By this, the plant 'seen' by the controller, i.e. the sequence f^{-1} and the real physical plant P, does not behave as nonlinear as the real plant alone, see as well Fig. 10.

The design of the controller $C(s)$ is further simplified when a dynamic feed-forward $C_{ff}(s)$ is added, see Fig. 11. If in the completely linear case with $f(\mathtt{u}^*) = \mathtt{u}^*$ the product $C_{ff}(s)\mathtt{r}(s)$ with reference $\mathtt{r}$ and $C_{ff}(s) = P^{-1}(s)$ is realizable, the system output $\mathtt{y}$ exactly equals the reference for vanishing disturbances $\mathtt{d}$ and $\mathtt{m}$ and exactly known plant model. Hence, the closed-loop controller $C(s)$ is only responsible for disturbance rejection in this ideal situation.

From different classical control synthesis methods loop-shaping approaches will be applied here. In a loop-shaping approach a controller $C(s)$ is determined such that in the case without feed-forward filter, see Eq. (29), the

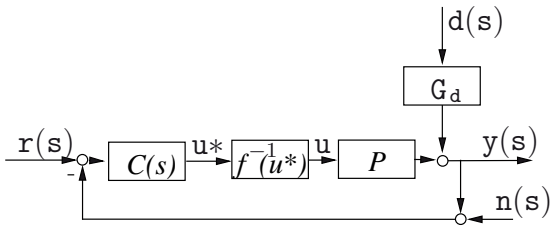

Figure 10. Closed loop with the physical control input signal u. The control input $\mathtt{u}^*$ calculated by the linear controller is nonlinearly transformed through f^{-1} inside the control system to determine u which is sent to the process. With this compensation of a Hammerstein-like nonlinear model the plant output y seen form the controller output $\mathtt{u}^*$ looks more linear.

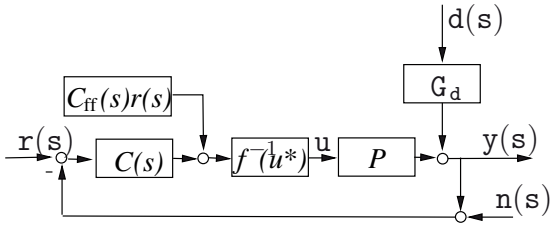

Figure 11. Closed loop with dynamic feed-forward filter.

frequency-dependent gain is $|T(j\omega)| \approx 1$ in the frequency range related to the reference signal r and low in the frequency range of the measurement noise m. Additionally, the gain of the sensitivity $|S(j\omega)|$ should be low to have a sufficient disturbance rejection. Most importantly, the controller must be such that the closed-loop system is asymptotically stable. In such a case the roots of all denominators of the closed-loop transfer functions, cf. Eq. (29), lie in the open left half complex plane. When transforming the transfer functions to the state space, these roots equal the eigenvalues of an appropriate $\boldsymbol{A}'$ matrix. For more information consult standard textbooks. With a feed-forward filter a faster response to set-pointed changes can be achieved and loop-shaping can concentrate on disturbance rejection.

Although the compensation of a nonlinear gain reduces the degree of nonlinearity, fluid flow systems remain inherently nonlinear. This will be reflected as well in other model parameters a_i, b_j and a variable system order

when different experiments are analyzed. A linear controller synthesized as indicated above will only work well if the system is not driven too far away from a constant setpoint around which the linearization is valid and if the control inputs are not high. Especially stability will only be guaranteed if this assumption holds. To account for nonlinear effects nonlinear methods, cf. Khalil (2002), can be used. They will be addressed later in this chapter in conjunction with Galerkin systems. Another approach is linear robust control. In robust control the uncertainty of a linear model is explicitly accounted for. Very good introductions to robust control are given in Skogestad and Postlethwaite (1996); Maciejowski (1994); Morari and Zafiriou (1989). A simple way to build a robust controller is to identify a family of linear models from different experiments related to different input signals or setpoints first as mentioned above, see Fig. 12.

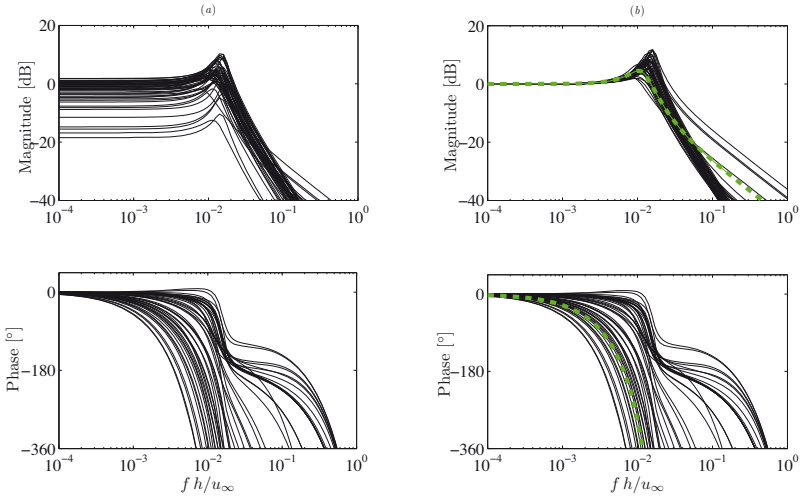

Figure 12. Left: Identified family of black-box models for the flow past a 2D bluff body for Re=46000 from Henning (2008). Right: The same model family with a compensated static gain and a nominal model depicted by a broken line. All plots are given as a function of a normalized frequency, i.e. as a function of the Strouhal number.

Now a controller is synthesized, loosely speaking, which is able to stabilize all models of the model family in the closed loop. Moreover, the

controller is chosen such that some requirements concerning performance are fulfilled. An automated way to do this is given by the theory of H_∞-control. In H_∞-control an optimization problem is solved to determine the controller thereby improving the overall goal for the 'poorest' situation.

All methods mentioned so far readily extend to the MIMO case. A MIMO flow control application based on robust control in the frequency domain can be found in Henning et al. (2008).

When working in the time instead of the frequency domain, controller synthesis is simplified for MIMO systems. For a plant

$$\dot{\boldsymbol{x}}(t) = \boldsymbol{A}'\boldsymbol{x}(t) + \boldsymbol{B}'\boldsymbol{u}(t) \tag{30}$$

minimization of

$$I = \frac{1}{2}\int_0^\infty (\boldsymbol{x}^T\boldsymbol{Q}\boldsymbol{x} + \boldsymbol{u}^T\boldsymbol{R}\boldsymbol{u})dt \tag{31}$$

leads to a well known state space controller

$$\boldsymbol{u}(t) = -\boldsymbol{K}\boldsymbol{x}(t) \tag{32}$$

where $\boldsymbol{K}$ is determined by the solution of a steady state quadratic Riccati equation. Beside providing an optimal solution by a closed-loop control law this Riccati controller guarantees robustness with respect to model uncertainties.

Another popular way to determine $\boldsymbol{K}$ is through pole placement. Substituting $\boldsymbol{u}$ by $-\boldsymbol{K}\boldsymbol{x}$ gives the equation of the closed loop

$$\dot{\boldsymbol{x}}(t) = (\boldsymbol{A}' - \boldsymbol{B}'\boldsymbol{K})\boldsymbol{x}(t) = \boldsymbol{A}'_c\boldsymbol{x}(t) \quad . \tag{33}$$

Stability of the steady state solution $\boldsymbol{x}_s = \boldsymbol{0}$ is given when all eigenvalues of $\boldsymbol{A}'_c$ stay in the open left half plane. For a scalar input u and an n-dimensional state vector n eigenvalues can be chosen, This fully determines $\boldsymbol{K}$ if the system is controllable. In the multi-input case free parameters in $\boldsymbol{K}$ can be chosen to fulfil further requirements concerning decoupling, eigenstructure assignment, minimization of control energy, etc.

State space controller assume the knowledge of the complete state $\boldsymbol{x}$. However, with

$$\boldsymbol{y}(t) = \boldsymbol{C}\mathrm{x}(t) + \boldsymbol{D}\boldsymbol{u}(t)$$

only a linear combination of the components of $\boldsymbol{x}$ (and of the control inputs) is available. To get a full state estimate a Luenberger observer or Kalman filter has to be applied, see the contribution by G. Tadmor in this book and Gelb (1986). For an extension to nonlinear systems, extended Kalman filters are recommended. Kalman filters perform better as well in the linear case as they explicitly take into account the noise which is prevalent in every real-live experiment.

3.3 Model predictive control

In the last two decades model predictive control (MPC) has been shown to be one of the most powerful and versatile control methods in process engineering. With the availability of constantly increasing computing power and the advent of highly efficient optimization methods MPC is within reach for the use in very fast flow control applications as well. This contribution gives an introduction into MPC and shows an example.

MPC is best explained by means of Fig. 13. The basic idea of MPC is to calculate future control inputs such that some performance criterion is optimized. In doing so, system constraints referring to states $\boldsymbol{x}$, outputs $\boldsymbol{y}$ and manipulated variables $\boldsymbol{u}$ are respected. For this purpose, the future control input $\boldsymbol{u}_f(t)$ is parameterized by, for example, piece-wise constant trajectories over a discrete-time horizon H_c. Usually, the sampling period

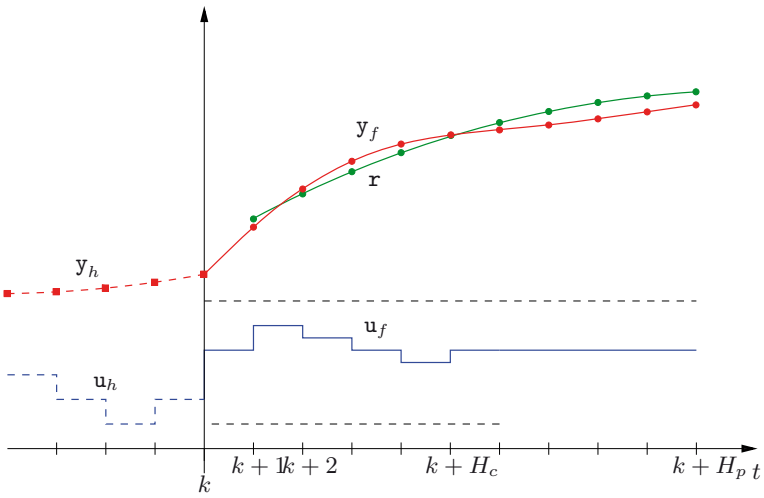

Figure 13. Basic scheme of MPC for a SISO system. Indices f and h refer to the future and the past, i.e. history, respectively. The reference signal $\mathtt{r}$ is specified starting from $k+1$, because the actual system output $\mathtt{y}(k)$ cannot be changed by the actual or future inputs.

h for the piece-wise constant control input is fixed. It coincides with the sampling period T of the model if a discrete-time model of the process is used. In the study of the von Kármán vortex street below it coincides with half the period of the flow. A variable sampling period, however, is possible as well, see e.g. Waldraff et al. (1997).

Let us assume that the actual discretized time instant is given by $t = k$. Hence, $t < k$ represents the past and $t > k$ the future. The actual control input for $t = k$, i.e. $\boldsymbol{u}(k) = \boldsymbol{u}_f(k)$, and future control inputs $\boldsymbol{u}_f(k+1)$, $\boldsymbol{u}_f(k+2), \ldots$ are now determined such that the system output $\boldsymbol{y}_f(k+i)$ is driven back to a reference trajectory $\boldsymbol{r}(k+i)$ for $H_1 \leq i \leq H_p$ in an optimal fashion. If a system with a pure time-delay d is considered, the output $\boldsymbol{y}$ will not be influenced by the actual input $\boldsymbol{u}(k)$ before $t = k + d$. In such cases, H_1 should be equal or larger than d. Even without time-delays, a $H_1 > 1$ might be beneficial for the overall performance.

Due to the piece-wise constant control input a finite parametric optimization problem results with optimization or design variables $\boldsymbol{u}_f(k), \boldsymbol{u}_f(k+1), \ldots$. The prediction horizon H_p is usually chosen (much) larger than the control horizon H_c in which control moves are allowed. A larger prediction horizon in comparison to the control horizon is beneficial for closed-loop stability. A thorough study shows that stability can be guaranteed if a terminal penalty or a terminal penalty and a terminal constraint are included, see Mayne et al. (2000) for a survey. A possible criterion or quality function may read without a terminal cost

$$J = \sum_{i=H_1}^{H_p} ||\boldsymbol{r}(k+i) - \boldsymbol{y}_f(k+i)||_{\boldsymbol{Q}} + \sum_{i=0}^{H_c} ||\boldsymbol{u}_f(k+i)||_{\boldsymbol{R}} \stackrel{!}{=} \min \quad , \qquad (34)$$

in which $\boldsymbol{Q}$ and $\boldsymbol{R}$ are symmetric weighting matrices used in the norms $||\cdot||$, i.e. $||\boldsymbol{z}||_{\boldsymbol{S}} = \boldsymbol{z}^T \boldsymbol{S} \boldsymbol{z}$. Both weights may depend on the time index $k+i$ as well. With the weights a different importance of manipulated values $\boldsymbol{u}_f(k+i)$ and future errors between reference $\boldsymbol{r}(k+i)$ and system output $\boldsymbol{y}_f(k+i)$ is accounted for. If changes in the control input $\Delta\boldsymbol{u}_f(k+i) = \boldsymbol{u}_f(k+i) - \boldsymbol{u}_f(k+i-1)$ are critical to avoid too large changes of the actuator amplitudes from one sampling instant to the next, these changes can be included in eq. (34) readily. Likewise, if the future control input for $t > k + H_c$ is not zero, its cost can be included as well. When constraints have to be considered, these can be dealt with via Lagrange operators or via penalty functions to name just two possibilities.

So far it was assumed that the optimal control input calculated after processing the measurement obtained at $t = k$ could be immediately applied at the same time instant. If the numerical burden is high, however, the measurements taken at $t = k$ are used to calculate the next control moves starting from $t = k + 1$. In such a case, the second summation in eq. (34) would start at $i = 1$.

In MPC, just the first control move $\boldsymbol{u}_f(k)$ of the calculated optimal input trajectory is applied to the plant. To react almost immediately when the

next measurement $\boldsymbol{y}$ for $t = k+1$ ist obtained, preparatory calculations can be done in the period from k to $k+1$. Then, the optimization starts from the beginning at the next sampling instant. By this, the influence of unknown disturbances and model errors is accounted for as these uncertainties show up in the next value of the measured output variable $\boldsymbol{y}(k+1)$. This repeated solution of an optimization problem has led to an alternative name of MPC, namely receding horizon optimal control.

In the general case, when the process model is nonlinear, a numerical solution of the optimization problem has to be done. This leads to a nonlinear model predictive controller (NMPC). A similar approach has to be taken for linear models in case of equality or inequality constraints which have to be met. This numerical solution, however, is responsible for the large numerical burden involved in solving (N)MPC problems. The beauty of the (N)MPC-method rests in its unifying framework. Irrespective of the kind of model, linear or nonlinear, continuous or discrete-time, SISO or MIMO, and irrespective of the optimization problem to be solved, unconstrained or constrained, the same principle can be used to derive a control signal.

To show the most simplest version of a MPC-scheme which leads to an explicit control law, a couple of assumptions will be made in the following. It is assumed that 1) the process model is given as a linear, discrete-time state-space model, 2) the plant output $\boldsymbol{y}(k)$ at time k will not directly depend on the control input $\boldsymbol{u}(k)$, i. e. there is no direct feed through, 3) the time for evaluating the control law obtained can be neglected, 4) no terminal terminal cost or terminal constraint is included, and 5) no constraints are considered.

MPC formulation for linear unconstrained problems As stated above every linear system can be described by a state-space model of the form

$$\boldsymbol{x}(k+1) = \boldsymbol{A}\boldsymbol{x}(k) + \boldsymbol{B}\boldsymbol{u}(k) \tag{35}$$

$$\boldsymbol{y}(k) = \boldsymbol{C}\boldsymbol{x}(k) \tag{36}$$

in which $\boldsymbol{x}, \boldsymbol{u}$ and $\boldsymbol{y}$ represent the internal state of the process, the control input and the process output, respectively. For ease of illustration, $\boldsymbol{D}$ is set to zero which is usually true in most applications.

Starting from time k, the future development of the process can be predicted exploiting Eq. (35). If a state prediction made at $t = k$ for $t = k + j$

is denoted by $\boldsymbol{x}(k+j|k)$, it follows

$$\begin{aligned}
\boldsymbol{x}(k+1|k) &= \boldsymbol{A}\boldsymbol{x}(k) + \boldsymbol{B}\boldsymbol{u}(k) \\
\boldsymbol{x}(k+2|k) &= \boldsymbol{A}\boldsymbol{x}(k+1|k) + \boldsymbol{B}\boldsymbol{u}(k+1) \\
&= \boldsymbol{A}^2\boldsymbol{x}(k) + \boldsymbol{A}\boldsymbol{B}\boldsymbol{u}(k) + \boldsymbol{B}\boldsymbol{u}(k+1) \qquad (37) \\
&\vdots \\
\boldsymbol{x}(k+H_p|k) &= \boldsymbol{A}^{H_p}\boldsymbol{x}(k) + \sum_{i=0}^{H_p-1} \boldsymbol{A}^i\boldsymbol{B}\boldsymbol{u}(k+H_p-1-i) \quad .
\end{aligned}$$

Hence, the future or predicted output for $k+j$ reads

$$\boldsymbol{y}_f(k+j) = \boldsymbol{y}(k+j|k) = \boldsymbol{C}\boldsymbol{A}^j\boldsymbol{x}(k) + \sum_{i=0}^{j-1} \boldsymbol{C}\boldsymbol{A}^i\boldsymbol{B}\boldsymbol{u}_f(k+j-1-i) \qquad (38)$$

in which $\boldsymbol{u}$ was replaced by $\boldsymbol{u}_f$ as future values of the control input are addressed. All future outputs will now be concatenated in $\boldsymbol{y}_p = (\boldsymbol{y}^T(k+1|k)\ \boldsymbol{y}^T(k+2|k) \ldots \boldsymbol{y}^T(k+H_p|k))^T$. Accordingly, $\boldsymbol{u}_p = (\boldsymbol{u}_f^T(k)\ \boldsymbol{u}_f^T(k+1)\ \ldots\ \boldsymbol{u}_f^T(k+H_c) \ldots \boldsymbol{u}_f^T(k+H_p))^T$ with $\boldsymbol{u}_f(k+j) = \boldsymbol{u}_f(k+H_c)$ for $j = H_c+1, H_c+2, \ldots, H_p$ to account for a constant manipulated variable for the last section of the prediction horizon H_p.

All future outputs inside the prediction horizon can now be written as

$$\boldsymbol{y}_p = \boldsymbol{A}_p\boldsymbol{x}(k) + \boldsymbol{B}_p\underline{\tilde{u}}_p \qquad (39)$$

with

$$\boldsymbol{A}_p = \begin{pmatrix} \boldsymbol{C}\boldsymbol{A} \\ \boldsymbol{C}\boldsymbol{A}^2 \\ \vdots \\ \boldsymbol{C}\boldsymbol{A}^{H_c} \\ \vdots \\ \boldsymbol{C}\boldsymbol{A}^{H_p} \end{pmatrix}$$

$$\boldsymbol{B}_p = \begin{pmatrix} \boldsymbol{C}\boldsymbol{B} & O & \ldots & O \\ \boldsymbol{C}\boldsymbol{A}\boldsymbol{B} & \boldsymbol{C}\boldsymbol{B} & \ldots & O \\ \vdots & \vdots & \ddots & \vdots \\ \boldsymbol{C}\boldsymbol{A}^{H_c}\boldsymbol{B} & \boldsymbol{C}\boldsymbol{A}^{H_c-1}\boldsymbol{B} & \ldots & \boldsymbol{C}\boldsymbol{B} \\ \boldsymbol{C}\boldsymbol{A}^{H_c+1}\boldsymbol{B} & \boldsymbol{C}\boldsymbol{A}^{H_c}\boldsymbol{B} & \ldots & \boldsymbol{C}\boldsymbol{B}+\boldsymbol{C}\boldsymbol{A}\boldsymbol{B} \\ \vdots & \vdots & \ddots & \vdots \\ \boldsymbol{C}\boldsymbol{A}^{H_p-1}\boldsymbol{B} & \boldsymbol{C}\boldsymbol{A}^{H_p-2}\boldsymbol{B} & \ldots & \sum_{i=0}^{H_p-H_c-1}\boldsymbol{C}\boldsymbol{A}^i\boldsymbol{B} \end{pmatrix}$$

$$\tilde{\boldsymbol{u}}_p = \begin{pmatrix} \boldsymbol{u}_f(k) \\ \boldsymbol{u}_f(k+1) \\ \vdots \\ \boldsymbol{u}_f(k+H_c) \end{pmatrix}$$

In the new variables $\boldsymbol{y}_p$, $\tilde{\boldsymbol{u}}_p$, the cost functional, Eq. (34), reads with $\boldsymbol{r}_p = (\boldsymbol{r}^T(k+1)\ \boldsymbol{r}^T(k+2)\ \ldots\ \boldsymbol{r}^T(k+H_p))^T$

$$\begin{aligned} J &= (\boldsymbol{r}_p - \boldsymbol{y}_p)^T \boldsymbol{Q}_p (\boldsymbol{r}_p - \boldsymbol{y}_p) + \tilde{\boldsymbol{u}}_p^T \boldsymbol{R}_p \tilde{\boldsymbol{u}}_p \\ &= (\boldsymbol{r}_p - \boldsymbol{A}_p \boldsymbol{x}(k) - \boldsymbol{B}_p \tilde{\boldsymbol{u}}_p)^T \boldsymbol{Q}_p (\boldsymbol{r}_p - \boldsymbol{A}_p \boldsymbol{x}(k) - \boldsymbol{B}_p \tilde{\boldsymbol{u}}_p) + \tilde{\boldsymbol{u}}_p^T \boldsymbol{R}_p \tilde{\boldsymbol{u}}_p \quad (40) \end{aligned}$$

The block diagonal matrices $\boldsymbol{Q}_p$ and $\boldsymbol{R}_p$ consist of $\boldsymbol{Q}$ and $\boldsymbol{R}$ matrices from Eq. (34) on the main diagonal if $H_1 = 1$. For $H_1 > 1$, the first entries in the main diagonal are zero. Equating $dJ/d\tilde{\boldsymbol{u}}_p = \underline{0}^T$ as a necessary and sufficient condition for an extremum yields for the future control input

$$\tilde{\boldsymbol{u}}_p = (\boldsymbol{B}_p^T \boldsymbol{Q}_p \boldsymbol{B}_p + \boldsymbol{R}_p)^{-1} \boldsymbol{B}_p^T \boldsymbol{Q}_p (\boldsymbol{r}_p - \boldsymbol{A}_p \boldsymbol{x}(k)) \quad . \qquad (41)$$

As no constraints are considered, a closed form of the control law is obtained. From $\tilde{\boldsymbol{u}}_p = (\boldsymbol{u}_f(k)\ \ \boldsymbol{u}_f(k+1)\ \ \ldots)$ only the first entry, i.e. $\boldsymbol{u}(k) = \boldsymbol{u}_f(k)$, is applied to the process. Then, the optimization starts from the beginning using the measurement $\boldsymbol{y}(k+1)$ to determine a new state $\boldsymbol{x}(k+1)$, and so forth. To obtain a state estimate, a model-based measuring technique such as a Kalman filter (Gelb, 1986) has to be applied if the full state vector $\boldsymbol{x}(k+1)$ cannot be measured.

As the following application of model predictive control will be limited to a nonlinear example exploiting a Galerkin system, the reader is referred to King et al. (2008); Muminovic et al. (2008); Gelbert et al. (2008) where a linear MPC is applied in experiments to a burner and a bluff body.

MPC formulation for constrained and /or nonlinear problems If constraints relating to the state $\boldsymbol{x}$, output $\boldsymbol{y}$, control input $\boldsymbol{u}$ or changes in the control input $\Delta\boldsymbol{u}$ have to respected, a closed solution of the optimization problem will be impossible. Numerical optimization methods have to be used then. With simple models, for example for the 3D bluff body considered in Muminovic et al. (2008), and appropriate numerical methods, for example active set methods, see Ferreau et al. (2007), we have already realized linear, constrained MPC with 8000Hz sampling frequency.

For nonlinear process models the prediction of the future behavior has to be done by a numerical integration. Moreover, the estimation of the gradient of the cost function with respect to future control moves is performed numerically too by repeating the prediction many times, each time slightly

changing one entry in the vector of future control inputs. Hence, even without constraints a huge numerical burden will be involved in nonlinear MPC. Today, this is still a limiting factor for flow control applications. Nevertheless, a nonlinear constrained simulation problem will be considered in the following to show the prospects of NMPC.

3.4 General nonlinear control

Much progress has been made in nonlinear control in the last decades. Any attempt to summarize this effort in this chapter is bound to fail. Therefore, the reader is referred to textbooks on nonlinear systems and control, see Khalil (2002); Isidori (2002), and to a contribution in which different nonlinear controllers were applied in a direct numerical simulation of a flow around a cylindrical cylinder based on a Galerkin system (King et al., 2005). Only one very simple nonlinear control method will be given here as it readily extends from the linear concepts introduced above.

If the state vector of a system $\boldsymbol{x}_1$ can be split up into a slowly changing part $\boldsymbol{x}_s$ and fast components $\boldsymbol{x}$, i.e. $\boldsymbol{x}_1 = [\boldsymbol{x}_s^T \ \boldsymbol{x}^T]^T$ and if the evolution equations can be given in the form

$$\dot{\boldsymbol{x}} = \boldsymbol{A}(\boldsymbol{x}_s)\boldsymbol{x} + \boldsymbol{B}\boldsymbol{u} \tag{42}$$

a linear parametrically varying (LPV-) system is given. Now, for fixed $\boldsymbol{x}_s$ pole placement can be used to find a state space controller, see Eq. (33).

4 Applications

In the collaborative research center 'Control of complex turbulent shear flows' at TU Berlin which was funded by the German Research Foundation the author and his group had the chance to test the above mentioned methods in numerous experimental tests. These involved the flow (and acoustics) for/with

- a backward-facing step in a SISO and MIMO setting
- a single 2-dimensional bluff body and a tandem configuration of two 2-dimensional bluff bodies
- a 3-dimensional Ahmed body
- various 2- and 3-dimensional wings with a flap as a high-lift device
- Tollmien-Schlichting instabilities over a profile
- noise-producing and/or stalling turbomachines
- mixers, a burner chamber, diffusors, and in a pipe.

From these examples only a small selection is considered here. A 2-dimensional bluff body is chosen to compare slope-seeking control, its extension with a

Kalman filter, robust control and phase control (see contribution of G. Tadmor in this book). Although not tested experimentally, the flow past a cylindrical cylinder, which is covered in several other chapters in this book, is included as well using nonlinear MPC and LPV-control.

Information about the other experimental closed-loop flow control studies can be found in the literature.

4.1 Two-dimensional bluff body - slope seeking

The flow separation behind bluff bodies, such as vehicles, shows complex space- and time-dependent topology which results in an increase in aerodynamic drag. A principle sketch of the investigated two-dimensional D-shaped body is shown in Fig. 14. The flow around the D-shaped body is governed by an absolute wake instability (Huerre and Monkewitz, 1990). This mechanism generates a von Kármán vortex street with an alternating sequence of vortices at characteristic frequencies. The natural flow is characterised by a short dead water region and alternating vortices in the vicinity of the base. Both are responsible for a low base pressure and thus for a high pressure-induced drag. The proposed active control strategy enforces a decoupling of the vortex formation in the shear layers and the wake by synchronising the roll-up of upper and lower shear layers. This delays the appearance of asymmetries in the wake flow and thus mitigates the wake instability. The dead water region is enlarged and the base pressure increases (Henning et al., 2007). Details, dimensions, etc. of the test section can be found in Pastoor et al. (2008).

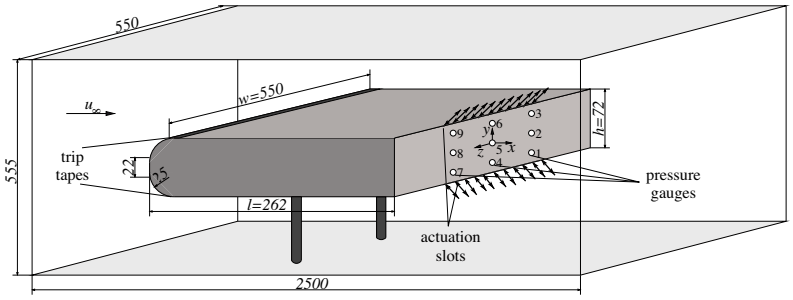

Figure 14. Sketch of the D-shaped body and the test section. All dimensions are in mm. Trip tapes are placed 30 mm downstream of the nose in order to trigger boundary layer transition.

A sinusoidal zero-mass actuation is applied by loudspeakers through

spanwise slots located at the upper and lower trailing edges. With this harmonic actuation the unstable processes of shear layer roll-up are triggered. By this means a maximum response of the flow can be generated with a minimum amount of input of energy. The actuation frequency f_a is related to natural instability frequencies of the flow. It should not be mistaken with the perturbation frequency $f_{sin} = 2\pi\omega_{sin}$ of the extremum controller used first.

The intensity of the actuation which will be modified in the following is characterised by the non-dimensional excitation momentum coefficient (Greenblatt and Wygnanski, 2000)

$$c_\mu = \frac{2\, s\, q_a^2}{h\, u_\infty^2} \quad , \tag{43}$$

in which q_a is the effective velocity of the actuation.

The base pressure is monitored by 3×3 difference pressure gauges mounted in three parallel rows on the rear end. The reference pressure is taken in front of the body. Four strain gauges are applied to the aluminium rods supporting the model for measurement of drag. The base pressure and drag are described by the non-dimensional coefficients

$$c_p(y,z,t) = \frac{\Delta p}{\rho\, u_\infty^2/2} \tag{44}$$

$$c_d(t) = \frac{f_x}{\rho\, u_\infty^2\, h\, w/2} \quad , \tag{45}$$

respectively. In the present work, Δp is the instantaneous pressure difference between a rear end-mounted pressure gauge and the reference pressure, ρ denotes the density, and f_x is the drag force. Spatially and spatially and temporally averaged base pressure across the stern are marked by $c_{pb}(t)$ and $\bar{c}_{pb}$, respectively.

The data acquisition and the implementation of the controllers are realized on a rapid prototyping hardware (*dSPACE-PPC1005* controller board). The sampling frequency is 1 000 Hz.

Fig. 15 (*a*) shows the steady-state map with the time-averaged base pressure coefficient as a function of the momentum coefficient at a constant Reynolds number $Re_h = 40\,000$ obtained from open-loop experiments in Henning et al. (2007). The Reynolds number is calculated with the body's hight h and free stream velocity u_∞. Both actuators operate in-phase with an optimal frequency $St_a = f_a\, h/u_\infty = 0.17$, which was indicated as the most effective actuation parameter for synchronisation of the shear layer development and for drag reduction in Henning et al. (2007). This steady-state

map is characterised by a plateau for $c_\mu \geq 7 \times 10^{-3}$. In order to achieve maximum base pressure with the minimum control input a slope-seeking controller with reference slope $f'_{ref} = 5$ is applied.

In the present study, the momentum coefficient is chosen as the input variable $u(t) = c_\mu(t)$, and the output is given by the spatially averaged base pressure coefficient $y(t) = c_{pb}(t)$. Information about the controller parameters are found in Henning et al. (2008).

The experimental data for a single operating point is shown in Fig. 15 (b–d). The controller starts at $c_\mu = 2 \times 10^{-3}$. The sinusoidal modifications

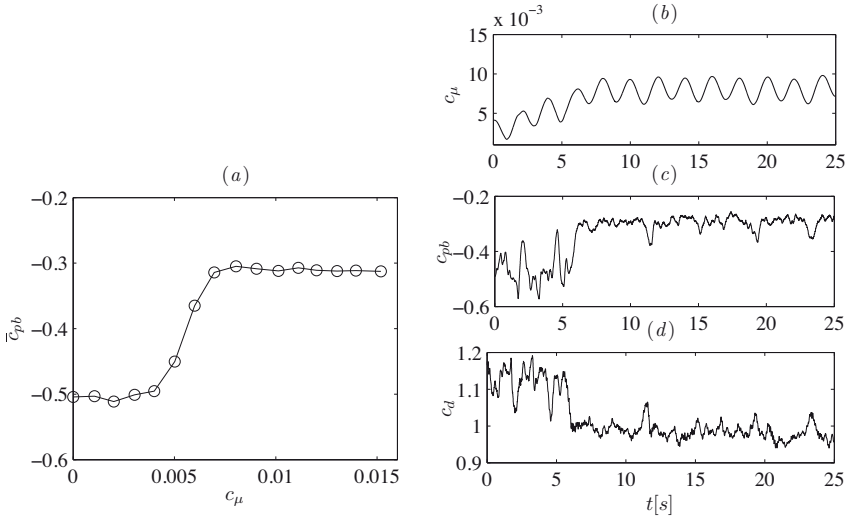

Figure 15. Steady-state map $\overline{c}_{pb} = f(c_\mu)$ obtained from open-loop experiments (a) and experimental implementation of slope-seeking feedback for optimal drag reduction of the D-shaped body (b–d). The controller adapts the actuation amplitude (b) until the maximum base pressure (c) has been reached and a maximum drag reduction of approximately 15% can be achieved. All experiments are performed at Reynolds number 40 000, in-phase forcing with a Strouhal number $t_a = 0.17$.

of c_μ are applied to obtain information about the local slope. According to the gradient, the actuation amplitude is raised until a state in front of the plateau is reached. This leads to a significant increase in the base pressure coefficient as shown in Fig. 15 (c), corresponding to the steady-state map. A reduction of the drag coefficient by 15% can be observed.

To show disturbance rejection of this controller, the Reynolds number is

increased continuously from 35 000 up to 60 000 in Fig. 16 *d*. Corresponding to the steady-state maps for various Reynolds numbers shown in Fig. 16 (*a*) the optimal actuation amplitude is automatically decreased with increasing Reynolds number. The experimental results in Fig. 16 (*b, c*) indicate that the desired averaged base pressure $c_{pb} = -0.3$ is maintained with the minimum control input.

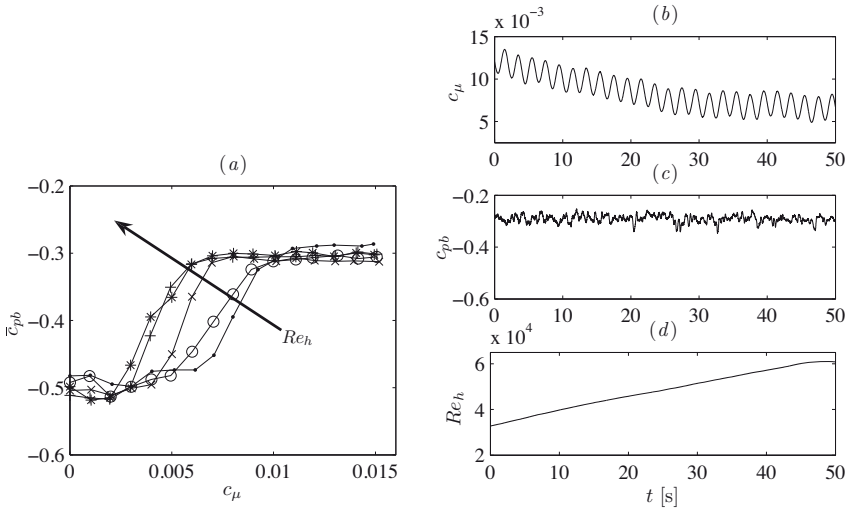

Figure 16. Slope-seeking feedback in an experiment with an increasing Reynolds numbers (*b–d*). Steady-state maps $\overline{c}_{pb} = f(c_\mu)$ are displayed (*a*) for various Reynolds numbers Re_h = 20 000 (•), 30 000 (∘), 40 000 (×), 50 000 (+), 60 000 (∗). These maps are used only to indicate the success of control. They are not required for the controller. Strouhal number of the in-phase forcing is $St_a = 0.17$.

The experimental results with the slope-seeking controller extended by the Kalman filter are shown in Fig. 17. The time delay is set to $n\Delta t = 2\,\pi/(3\,\omega_{sin})s = 660\Delta t$ with sampling time $\Delta t = 0.001$s. An almost three times faster response is observed compared to the classical approach due to the fast estimation of the local gradient $\hat{f}'$, see Fig. 17 (*d*).

4.2 Two-dimensional bluff body - robust control

To identify a low dimensional dynamical model different experiments with different actuation signals are run. In this case, the actuation am-

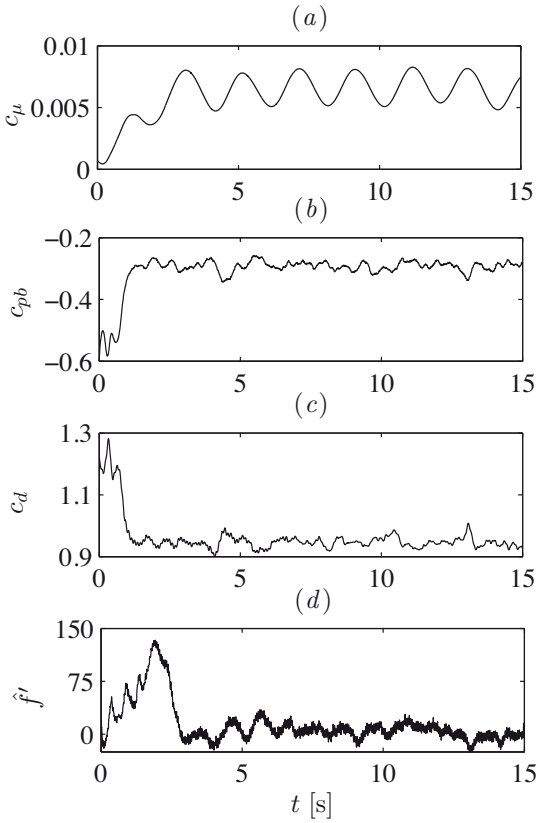

Figure 17. A fast extended Kalman filter algorithm is used to estimate the current slope (d) of the steady-state map. Thus the slope-seeking controller can achieve the optimal momentum coefficient faster (a) which leads to an increase in base pressure (b) and a reduction of the drag coefficient (c) of the D-shaped body. Harmonic in-phase actuation with $St_a = 0.17$ at $Re_h = 40\,000$ is applied.

plitude $\mathtt{u}(t) = \hat{\mathtt{u}}$ is switched on/off to/from different levels of $\hat{\mathtt{u}}$. Each experiment is identified with a linear black-box model. A Bode plot of all models found for a certain Reynolds number is given in Fig. 12. For a truly linear system all identified models should be equal. The spread in the Bode plots seen, however, is an indication of the nonlinearity of the plant.

For the gain of all identified models in the left panel of Fig. 12 a nonlinear

static relationship $f(\cdot)$ with respect to the input amplitude $\hat{\mathtt{u}}$ is found. This knowledge can be used to reduce the uncertainty in the model description as outlined above. The result is given in right panel of Fig. 12. From the latter a so-called nominal model of second order with time-delay T_0

$$T_2^2\ddot{y}(t) + T_1\dot{y}(t) + y(t) = K\big(u(t-T_0) + T_d\dot{u}(t-T_0)\big) \tag{46}$$

is obtained, see as well Fig. 12. Instead of using parameters a_i and b_j, time constants and a power of a time constant are introduced here. With respect to the model parameters K, T_0, T_1, T_2 and T_d this nominal model shows the smallest distance to all other models identified. The non-dimensionalized parameterized uncertainties are given by

$$\begin{aligned} K &= 1 \\ T_0 u_\infty/h &= 68.65(1+0.98\delta) \\ T_1 u_\infty/h &= 9.19(1+0.73\delta) \\ T_2 u_\infty/h &= 13.76(1+0.32\delta) \\ T_d u_\infty/h &= 5.49(1+1.0\delta) \end{aligned} \tag{47}$$

with $-1 \le \delta \le 1$.

Although the flow in the recirculation region behind the body is highly complex, a very simple nominal model is obtained relating actuation amplitude $\mathtt{u}(t)$ with mean base pressure $\mathtt{y}(t) = c_{Pb}(t)$.

To increase the bandwidth of the closed loop with respect to reference signals a dynamic pre-filter $G_{ff}(s)$ is included as well, see King et al. (2005); Henning (2008) for more details.

Based on the nominal model and the uncertainty description a robust controller is synthesized using the MATLAB® robust control toolbox. With this robust controller the behavior of the controlled system is tested in wind tunnel experiments with respect to tracking response and disturbance rejection. Fig. 18 shows the tracking response of the closed-loop after stepwise changes of the reference command. A good tracking performance can be observed. High-frequency disturbances are not rejected because of both the system's inherent limited tracking dynamics and the requirement of robustness giving a limitation of the closed-loop performance. A main advantage of closed-loop control in comparison to open-loop control is disturbance rejection. To demonstrate the robustness of the closed-loop control the Reynolds number is varied in the same experiment from 7×10^4 to 4×10^4. The setpoint-tracking capability is not effected by this disturbance which is unknown to the controller. More information can be found in Henning and King (2005); Henning (2008).

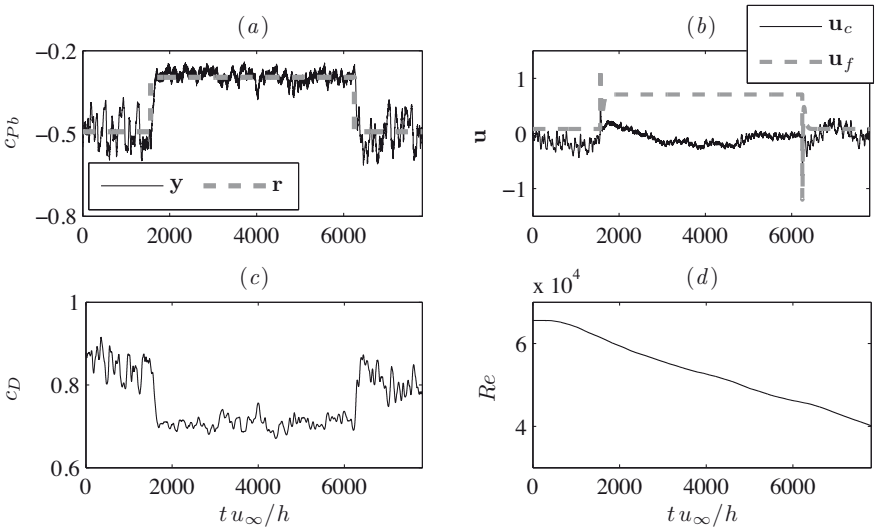

Figure 18. Robust control of the base pressure $y = c_{Pb}$ while changing the setpoint r and the Reynolds number Re from Henning (2008). The obtained drag c_D is given for reference. The control input $u(t)$ is given by the sum of the fast feed-forward term u_f and the controller output u_c.

This robust controller is significantly faster than an extremum- or slope-seeking controller. This has to be payed for, however, by an increased effort in identifying the model family and running the approriate identification experiments.

The application of the robust controller suffers from rather large values of the manipulated variable. Hence, another idea to save energy is to reject the detrimental alternate vortex shedding and to generate a synchronized vortex shedding in the near wake, instead. This can be accomplished by one actuation slot only which is synchronized with naturally occurring vortices of the opposite side. By this, see contribution of G. Tadmor in this volume or Pastoor et al. (2008), the same control success as with the robust controller can be achieved with a reduction of the spend control energy of 40%.

4.3 MPC, energy-based and LPV-control of the cylinder wake

We consider the 3-dimensional Galerkin system including a shift mode introduced by B.R. Noack, see chapter by Noack et al. and Noack et al.

(2003), with $a_1 = A\cos\Phi$, $a_2 = A\sin\Phi$

$$\begin{bmatrix} \dot{A} \\ \dot{\Phi} \\ \dot{a}_3 \end{bmatrix} = \begin{bmatrix} (\sigma_r - \beta a_3)A \\ \omega + \gamma a_3 \\ \alpha A^2 - \sigma_3 a_3 \end{bmatrix} + \begin{bmatrix} g_c\,\cos(\Phi-\theta) \\ -(g_c/A)\,\sin(\Phi-\theta) \\ 0 \end{bmatrix} \mathtt{u} \quad . \tag{48}$$

Several nonlinear control synthesis methods have been applied in King et al. (2005) to dampen the von Kármán vortex street. Although these formally derived methods successfully controlled the wake, none was better than a formerly proposed controller which is build upon physical insight of the system, cf. Gerhard et al. (2003). One of the controller tested in King et al. (2005) is based on an LPV-point of view. It will be given below. However, the physically motivated controller will be reviewed first.

The original work (Gerhard et al., 2003) was a proof-of-concept study showing that an empirical Galerkin model derived from natural flow data can also be employed for an actuated flow. One conclusion was that the system should stay in the region of validity of the low dimensional model. Following this argument, more classical nonlinear methods of controller synthesis were ruled out in Gerhard et al. (2003), as it was expected that these methods do not preserve the range of model validity. A simple energy-based controller was proposed, instead, with $\mathtt{u} = -\mathtt{u}_0$ if $g_c\cos(\Phi-\theta) > 0$, and $\mathtt{u} = +\mathtt{u}_0$ otherwise. With a rather complicated formula, see as well (Tadmor et al., 2003), the amplitude $\mathtt{u}_0$ was determined once every period in agreement with a desired decay rate of the amplitude A. The mean impact of the force on the phase Φ was small because of the sign-change of the angle force-term $g_c\sin(\Phi-\theta)$, see Eq. (48), during the time of constant force direction.

With this control law, the turbulent kinetic energy, expressed as $\sum_{i=1}^{N}\langle a_i^2\rangle/2$, could not only be reduced for the model used in the controller synthesis itself, with 3 POD-modes. The very same control law synthesized with a third order system reduces also the energy in higher-order Galerkin modes in the real system, since the higher harmonics get their energy from the suppressed first harmonics. This was shown by applying the controller to Galerkin approximations with $N = 7$ and $N = 9$ states. Finally, the complete system was controlled in a DNS study. A nonlinear observer (Zeitz, 1987) was build up using the measurement device shown in Fig. 19 to implement the control in the DNS. The gain of the nonlinear observer was determined so that the linearized dynamics of the state-space estimation error was stable.

In the following, a new and simpler version of this energy-based control is proposed. If $g_c\cos(\Phi-\theta) \geq 0$, the mean influence of the control on $\dot{A}$ during half a period $T/2$ can be approximated, using $\phi \approx \omega t$ and $\omega T \approx 2\pi$,

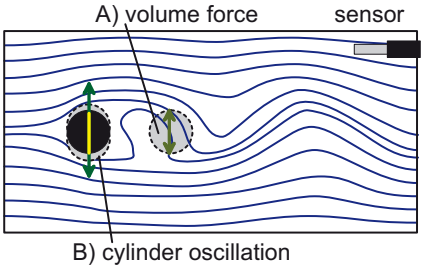

Figure 19. Principal sketch of the actuated cylinder wake. The figure displays the streamlines of the natural flow around a circular cylinder with diameter $D = 1$ (solid circle). Actuation is provided by transverse cylinder oscillation or by a transverse volume force in the grey circle. The flow state is sensed with a hot-wire anemometer, located at a typical position. Success of control is monitored in the observation region $-5 < x < 15$, $-5 < y < 5$, with $x = y = 0$ in the center of the cylinder, see Fig. 21 as well.

by

$$\frac{2g_c}{2\pi}\int_{-\pi/2}^{\pi/2}\cos(\Phi-\theta)d(\Phi-\theta)=\frac{2g_c}{\pi} \quad . \tag{49}$$

Replacing $g_c\cos(\Phi-\theta)$ in the first equation of (48) by the mean influence $2g_c/\pi$, and demanding that

$$(\sigma_r-\beta a_3)A+\mathtt{u}_0\frac{2g_c}{\pi}=-kA \quad ,$$

with a decay rate $-k$, yields the control

$$\mathtt{u}_0=\frac{\pi}{2g_c}\Big(-k-\sigma_r+\beta a_3\Big)A \quad . \tag{50}$$

For $\cos(\Phi-\theta)<0$ an opposite sign is needed. This finally leads to the new energy-based (eb) control

$$\mathtt{u}_{eb}=-\frac{\pi A(k+\sigma_r-\beta a_3)}{2g_c}\,\mathrm{sign}\{\cos(\Phi-\theta)\} \quad . \tag{51}$$

The LPV-character of the system is better seen when it is further transformed using $b_1 = r\sin(\Phi-\theta)$ and $b_2 = r\cos(\Phi-\theta)$

$$\begin{bmatrix}\dot b_1\\ \dot b_2\\ \dot a_3\end{bmatrix}=\begin{bmatrix}(\sigma_r-\beta a_3)b_1+(\omega+\gamma a_3)b_2\\ -(\omega+\gamma a_3)b_1+(\sigma_r-\beta a_3)b_2\\ -\sigma_3 a_3+\alpha(b_1^2+b_2^2)\end{bmatrix}+\begin{bmatrix}0\\ g_c\\ 0\end{bmatrix}\mathtt{u} \quad . \tag{52}$$

As the shift mode $a_3(t)$ is only slowly varying the first two equations make up an LPV-system. In a pole placement approach the poles of the closed-loop are placed at each sampling instant such that in an energy optimal sense the unstable poles of the open-loop system are mirrored at the imaginary axis and shifted 0.001 to the left. The control law can be written as

$$\mathtt{u}_{LPV} = -\frac{A(t)}{g_c}\Big(K_{LPV1}(a_3(t))\cos(\Phi-\theta) - K_{LPV2}(a_3(t))\sin(\Phi-\theta)\Big) \quad (53)$$

where K_{LPV1} and K_{LPV2} are more intricate functions of $a_3(t)$.

Applying this controller in a direct numerical simulation (DNS) with a code provided by M. Morzyński resulted in an 24% post-transient reduction of the turbulent kinetic energy compared to the physically proposed controller which achieved 32%. However, better results are obtained with a nonlinear model predictive controller.

To test the NMPC the direct numerical simulations are performed on a grid with 8712 nodes. For state estimation based on the velocity measurement depicted in Fig. 19, an extended Kalman filter is applied. As the Galerkin system is nonlinear, integration of the system equations for prediction and the solution of the extended Kalman filter equations has to be done numerically. Likewise, a numerical optimization routine is used to minimize the cost functional. In this example not a constant reference trajectory for the velocity measured is used. Instead a reference trajectory for the first mode amplitude is given. A very simple cost functional is used here instead of Eq. (34)

$$J = \int_t^{t+H_p} e^2(l)dl \qquad \text{with} \qquad e(t) = r(t) - \hat{a}_1 \quad , \qquad (54)$$

i.e. the control effort is neglected. The scalar reference $r(t)$ is chosen as a sinusoidal signal with exponentially decreasing amplitude. This choice is motivated by the limited validity of the low dimensional Galerkin system. The variable $\hat{a}_1(t)$ denotes the estimated value of the state variable $a_1(t)$. To make the optimization problem easier, we use even more physical knowledge about the process. From the physically motivated controller it is known that good results are obtained when a piece-wise constant u is synchronized with $cos(\Phi-\theta)$. This knowledge is exploited here as well. No arbitrary sampling period h, see Fig. 13, is chosen, but one that exactly matches the physics of the process. Inside a sampling period, u_f is chosen to be constant.

To respect the validity of the model, the calculated future control inputs are constraint to $|u_f(t+l)| < 0.1$. For more details see Aleksic et al. (2008). A comparison in Fig. 20 shows the superiority of NMPC which is significantly faster than energy-based control and leads to a recirculation zone of

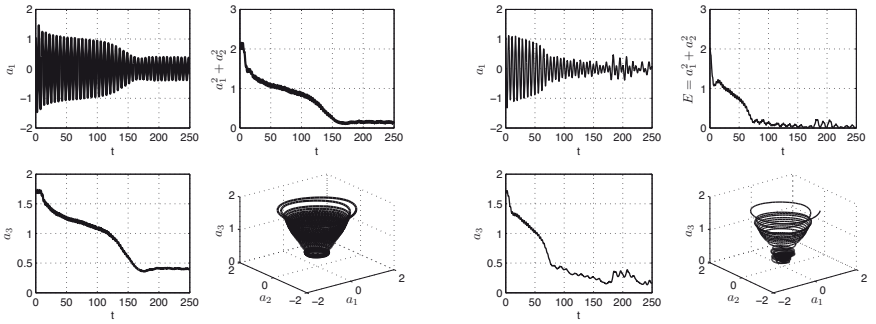

Figure 20. Fourier coefficients a_i obtained in a closed-loop controlled DNS by applying the controller based on physical intuition from Gerhard et al. (2003) (left) and NMPC (right). State estimation is done with an extended Kalman filter. The success of the control is observed by $a_1^2 + a_2^2$ which describes the major part of the turbulent kinetic energy.

length 5.2 in contrast to 4.1 for the energy-based control, see Fig 15. With no other controller using the very same measurement information and the same actuation concept such good results were found in King et al. (2005). Even with the improved versions of the backstepping and Lyapunov-based controllers in Aleksic et al. (2007), a poorer performance was obtained. Fig. 21 shows a plot of the streamlines of the unactuated and the actuated case with the NMPC controller at t=120. The damping effect of the actuation and the significant mitigation of the instability is clearly visible in the observation region.

5 Conclusions

Comparing the different controllers proposed a hierarchy concerning robustness, velocity and modeling effort can be given, see Fig. 22.

Physically motivated controllers can be very fast and, certainly depending on the application, rather robust when strong and reproducible coherent events take place. A rational exploitation of these phenomena necessitates a good physical understanding of the process as in the case of the phase control shown in the part of G. Tadmor or needs a good model as the Navier-Stokes equation derived Galerkin model of the 2D flow around a circular cylinder treated above.

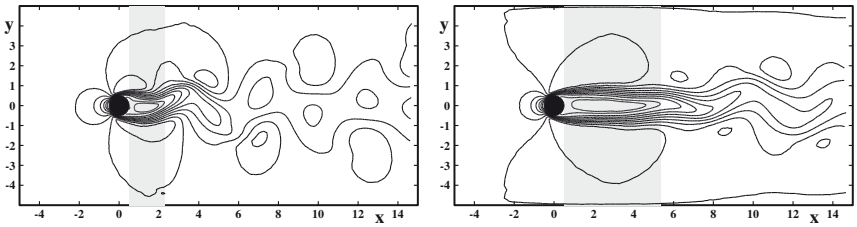

Figure 21. Left: Unactuated flow. Right: Actuated flow with an NMPC controller shown for $t = 120$. The figures display isocontours of the streamwise velocity component U. Negative values are indicated by thinner curves and show the extent of the recirculation region. The shaded area depicts the length of the recirculation zone.

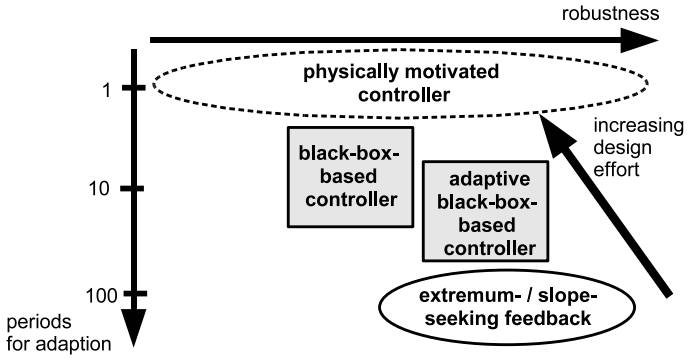

Figure 22. Time scales, robustness and required modeling effort of different controllers.

In many classical controllers, models of a process are only used during synthesis of the controller. In contrast, the phase control and MPC exploit a process model inside the algorithm. As an optimization problem over a future horizon is considered in MPC, there are no restrictions concerning the variables which are used to describe the success of control as long as they can be calculated by that model. Very different criteria can be formulated, combining different aspects at the same time. Moreover, when enough computing power is available, equality and inequality constraints can be included in the optimization in a straightforward manner. With no

other control technique this practically very important issue can be dealt with so easily. However, as the name tells, MPC is based on a model. If this model is not derived theoretically, it has to be identified based on experimental data in a black-box manner. The time needed for this step should not be underestimated. In the MPC approaches shown here, robustness is not dealt with explicitly. If this has to be done, the computational burden increases significantly.

Robustness issues can be addressed with more classical techniques, such as a H_∞-control. Numerous experimental tests with different flow configurations have shown their good performance.

For all approaches mentioned so far as well as for the slow but easy to apply extremum-seeking control methods the limitations or difficulties often do not arise from control engineering (when you know this subject) but from the search of appropriate actuators and sensors to influence the flow and get informative information, respectively.

Bibliography

K. Aleksic, R. King, B.R. Noack, O. Lehmann, M. Morzynski, and G. Tadmor. Nonlinear flow control using a low dimensional galerkin model. In *X Triennial International SAUM Conference on Systems, Automatic Control and Measurements*, Nis, Serbia, 2007.

K. Aleksic, R. King, B.R. Noack, O. Lehmann, M. Morzynski, and G. Tadmor. Nonlinear model predictive control based on a low dimensional model of fluid flow. In *Int. Conf. on Jets, Wakes and Separated Flows 2008*, Berlin, Germany, 2008.

K.B. Ariyur and M. Krstic. *Real-Time Optimization by Extremum-Seeking Control*. John Wiley & Sons, Hoboken, 2003.

J.-F. Beaudoin, O. Cadot, J.-L. Aider, and J.-E. Wesfried. Drag reduction of a bluff body using adaptive control methods. *Physics of Fluids*, 18: 085107, 1–10, 2006.

R. Becker, R. King, R. Petz, and W. Nitsche. Adaptive closed-loop separation control on a high-lift configuration using extremum seeking. *AIAA Journal*, 45:1382–1392, 2007.

H.J. Ferreau, P. Ortner, P. Langthaler, L. del Re, and M. Diehl. Predictive control of a real-world diesel engine using an extended online active set strategy. *Annual Reviews in Control*, 31(2):293–301, 2007.

M. Garwon, F. Urzynicok, L. H. Darmadi, G. Bärwolff, and R. King. Adaptive control of separated flows. In *Proc. of the ECC 2003*, Cambridge, 2003.

A. Gelb. *Applied Optimal Estimation*. The M.I.T. Press, Cambridge, 1986.

G. Gelbert, J.P.Moeck, M.R. Bothien, R. King, and C.O. Paschereit. Model predictive control of thermoacoustic instabilities in a swirl-stabilized combustor. *AIAA Paper* 2008-1055, 46th AIAA Aerospace Sciences Meeting and Exhibit, 2008.

J. Gerhard, M. Pastoor, R. King, B. R. Noack, A. Dillmann, M. Morzynski, and G. Tadmor. Model-based control of vortex shedding using low-dimensional Galerkin models. *AIAA Paper* 2003-4262, 2003.

D. Greenblatt and I. Wygnanski. The control of flow separation by periodic excitation. *Prog. Aerospace Sci.*, 36:487–545, 2000.

L. Henning. *Closed-loop control of separated shear flows by active means (in german).* PhD thesis, TU Berlin, `opus.kobv.de/tuberlin/volltexte/2008/1861/`, Berlin, 2008.

L. Henning and R. King. Drag reduction by closed-loop control of a separated flow over a bluff body with a blunt trailing edge. In *Proc. of the 44th IEEE Conference on Decision and Control and European Control Confernce, CDC-ECC'05*, Seville, Spain, 2005.

L. Henning, M. Pastoor, R. King, B.R. Noack, and G. Tadmor. Feedback control applied to bluff body wake. In R. King, editor, *Active Flow Control*, pages 325–228, Springer-Verlag, Berlin, 2007.

L. Henning, G. Feuerbach, R. Muminovic, A. Brunn, W. Nitsche, and R. King. Extensions of adaptive slope-seeking for active flow control. *Proc. IMech, Part I: J. Systems and Control Engineering*, pages 309–322, 2008.

P. Huerre and P. A. Monkewitz. Local and global instabilities in spatially developing flows. *Annual Review Fluid Mechanics*, 22:473–537, 1990.

A. Isidori. *Nonlinear Control Systems.* Springer, 2002.

H.K. Khalil. *Nonlinear Systems.* Prentice Hall, 2002.

R. King, R. Becker, M. Garwon, and L. Henning. Robust and adaptive closed-loop control of separated shear flows. *AIAA-Paper* 2004-2519, 2004.

R. King, M. Seibold, O. Lehmann, B.R. Noack, M. Morzynski, and G. Tadmor. Nonlinear flow control based on a low dimensional model of fluid flow. In Meurer et al., editor, *Lecture Notes in Control and Information Science*, volume 322, pages 365–386. Springer, 2005.

R. King, R. Becker, G. Feuerbach, L. Henning, R. Petz, W. Nitsche, O. Lemke, and W. Neise. Adaptive flow control using slope seeking. In *14th IEEE Mediterranean Conference on Control Automation*, Ancona, 2006.

R. King, K. Aleksic, G. Gelbert, N. Losse, R. Muminovic, A. Brunn, W. Nitsche, M. R. Bothien, J. P. Moeck, C. O. Paschereit, B. R. Noack, U. Rist, and M. Zengl. Model predictive flow control. *AIAA Paper* 2008–3975, *Proc. of the 4th AIAA Flow Control Conference*, Seattle, 2008.

M. Krstic and H.-H. Wang. Stability of extremum seeking feedback for general nonlinear dynamic systems. *Automatica*, 36:595–601, 2000.

L. Ljung. *System Identification: Theory for the User*. Prentice Hall, Englewood Cliffs, New Jersey, 1999.

J. M. Maciejowski. *Robust Process Control*. Addison-Wesley, Wokingham, England, 1994.

D. Q. Mayne, J. B. Rawlings, C. V. Rao, and P. O. M. Scokaert. Constrained model predictive control: Stability and optimality. *Automatica*, 36:789–814, 2000.

M. Morari and E. Zafiriou. *Robust Process Control*. Prentice-Hall, Englewood Cliffs, New Jersey, 1989.

I. S. Morosanov. Method of extremum control. *Automation Remote Control*, 18:1077–1092, 1957.

R. Muminovic, L. Henning, R. King, A. Brunn, and W. Nitschev. Robust and model predictive control for a generic car model. *AIAA Paper* 2008-3859, 4th AIAA Flow Control Conference, 2008.

B.R. Noack, K. Afanasiev, M. Morzynski, G. Tadmor, and F. Thiele. A hierarchy of low-dimensional models of the transient and post-transient cylinder wake. *J. Fluid Mechanics*, 497:335–363, 2003.

M. Pastoor, L. Henning, B.R. Noack, R. King, and G. Tadmor. Feedback shear layer control for bluff body drag reduction. *J. Fluid. Mech.*, 608: 161–196, 2008.

S. Skogestad and I. Postlethwaite. *Multivariable Feedback Control - Analysis and Design*. John Wiley & Sons, Chichester, England, 1996.

G. Tadmor, B.R. Noack, A. Dillmann, J. Gerhard, M. Pastoor, R. King, and M. Morzynski. Control, observation and energy regulation of wake flow instabilities (paper 909). In *Proc. of the 42nd IEEE Conference on Decision and Control*, pages 2334–2339, Maui, USA, 2003.

W. Waldraff, R. King, and E.D. Gilles. Optimal feeding strategies by adaptive mesh selection for fed-batch bioprocesses. *Bioprocess Engineering*, 17:221–227, 1997.

T. Weinkauf, H.-C. Hege, M. Schlegel, and A. Dillmann. Coherent structures in a transitional flow around a backward facing step. *Phys. Fluids*, 15: S3, 2003.

M. Zeitz. The extended Luenberger observer for nonlinear systems. *Systems and Control Letters*, 9:149–156, 1987.